University of Stavanger

FACULTY OF SCIENCE AND TECHNOLOGY

MASTER'S THESIS

Study programme/specialisation:	Spring semester, 2021
Petroleum Engineering/ Reservoir Engineering	Open

Author: Jan Stychlerz

Programme coordinator:

Supervisor(s): Pål Østebø Andersen

Mohammad Ghasemi

Title of the master's thesis:

Evaluation of asphaltene deposition during CO2 enhanced oil recovery

Credits: 30 ECTS

Keywords: CO2 injection, EOR, asphaltene deposition, CCS, Asphaltene onset pressure, Equation of state	Number of pages: 56 Stavanger, 27/07/2021

Title page for the master's thesis
Faculty of Science and Technology

Internal

Abstract

Over the years carbon dioxide has been gaining immense attention. Being one of the main greenhouse gases, it contributes to the increment of the global temperature more and more significantly. Existing as a by-product of fuel combustion, technological industries productions, or as a part of natural gas – it is ubiquitous. But CO2 has been found to surprisingly effectively interact with the crude oil in the reservoir, making it an interesting agent in enhanced oil recovery processes. Injecting CO_2 as the gas or supercritical fluid into the reservoir has some drawbacks though. One of them is the precipitation of asphaltenes from a crude oil-CO2 mixture. This can lead to severe complications in flow in porous media like reduced permeability, ultimately leading to a decline in the production or injectivity. The study of carbon dioxide volume-pressure influence on the hydrocarbons in terms of asphaltene precipitation is the primary objective of this work. Main controls of the process will be deeply studied and modeled to get a better understanding of CO_2 influence. With this study, we want to study the main controls of the asphaltene precipitation during CO_2 injection and explore the dependence of the pressure, temperature, and gas content on the process. Series of laboratory measurements performed enabled us to build an accurate PVT model in PVTsim, that can predict asphaltene precipitation in various conditions. Hopefully, this work can deliver a better understanding of the potential asphaltene onset in the CO_2-oil mix, making the CO_2-EOR and CCS projects more feasible in the future.

Internal

Nomenclature

A - Soave-Redlich-Kwong equation parameter
a - Soave-Redlich-Kwong equation correction for at the tractive potential of molecules
a_c - Soave-Redlich-Kwong equation parameter
B - Soave-Redlich-Kwong equation parameter
b - Soave-Redlich-Kwong equation correction for volume
GOR – Gas oil ratio [scf/bbl]
n_g – number of moles of gas [-]
n_o - number of moles of fluid [-]
P - Pressure [bar]
P_b – Saturation pressure [bar]
P_c – Critical pressure [bar]
R – Universal gas constant $R = 8{,}314\ \frac{J}{mol \cdot K}$
T – Temperature [K]
T_c - Critical temperature [K]
V – Molar volume [m^3/mol]
v – Total volume [m^3]
z – compressibility factor [-]
ω – acentric factor [-]

Internal

Acknowledgments

I would like to express:

Extreme gratitude to my supervisors Pål Østebø Andersen and Mohammad Ghasemi for their help and guidance.

Special thanks to Halstein Bjørsvik for his mentoring and laboratory assistance.

I would also like to thank

my Parents, Brother and Grandparents for their love and support.

to Adam and Rocco, for reminding me what really matters

Twin peaking, highs and lows

Internal

Table of Contents

Internal

Table of Figures

Internal

Introduction

With the world introducing more and more strict rules regarding CO_2 emissions to the atmosphere, the oil and gas companies are under increasing pressure of becoming carbon neutral while producing fossil fuels. One of the approaches to achieve this scenario is by injecting by-product carbon dioxide back into the reservoir. Not only it helps meet the emission goals, but also it is a proven method to boost productivity by either oil-viscosity reduction or oil swelling (immiscible flooding), or by shifting thermodynamical and changing fluid behaviour (miscible flooding). Obviously, it is not the easiest and versatile method, as not every reservoir can efficiently produce while large amounts of this gas are introduced to the petroleum system. One of the common problems is asphaltene precipitation that is triggered while the oil-gas-CO_2 system mixes. Precipitated solids can significantly influence reservoir permeability or in the worst case even clog the pores, leading to trapped hydrocarbons and originate of non-productive zones, ultimately reducing field productivity. Thus it is necessary to study how the system is developing under increasing carbon dioxide content. Adyani, Daud, Darman, Memon, Khan, and Jamaluddin [1] established a systematic approach and workflow process for evaluating CO_2 miscibility criteria and asphaltene precipitation propensity based on the samples from a reservoir of a field located in the South China Sea. They have also calculated asphaltene content based on the area covered by probable particles under the high-pressure microscope. However, from the experience of the lab staff, this seems to be an inaccurate approach. As the asphaltene onset pressure is within close range to saturation pressure, gas bubbles might appear, which can be easily interpreted as precipitating solids on the image. Lei, Pingping, Ying, Jigen, Shi and Aifang [2] came up with a thermodynamic model that is incorporating the complexity of asphaltenes and can yield accurate predictions on the precipitation based on pressure, temperature, and volume (PVT) data. Zanganeh, Ayatollahi, Alamdari, Zolghadr, Dashti, and Kord [3] performed similar studies, but they have focused on visual studies of microscopic images. They have also proposed the so-called potential of deposition. With this work, we wanted to come up with an asphaltene precipitation forecasting model based on lab studies on the pressurized oil sample and see what the trends and main parameters influencing the model are. It has been noticed in the previous works that the increasing CO_2 content in the mixture is scaling up the asphaltene onset pressure (AOP). During the gas injection process, at some point, the stream mixes with the fluid in-place. Higher AOP can lead to early solid precipitation and ultimately ending up with problems mentioned above. The temperature drop might also raise the AOP. By combining laboratory measurements with state-of-art PVTsim modelling software, we will investigate those relations.

Internal

Theoretical background

1.1 Chemical properties

1.1.1 Crude Oil

Crude oil is a natural mixture of various components. It is mostly consisting of different types of hydrocarbons such as alkanes, naphthenes, or aromatics. Other compounds are sulphur, nitrogen, and oxygen. Hydrocarbons make up from 30% to 100% of the total crude oil composition. [4]. One of the most popular classifications of the components in the oil is the SARA classification (which stands for Saturates, Aromatics, Resins, and Asphaltenes). Saturates are linear, branched, and cyclic saturated, non-polar hydrocarbons. Aromatics are more polarizable and are made out of one or more aromatic rings. The last two parts which are resins and asphaltenes can be distinguished by their polar substituents. The one major difference is that asphaltenes are insoluble in an excess of heptane/pentane, while resins are fully miscible with them[5]

1.1.2 Asphaltenes

Asphaltene constituents (sometimes referred to as solid hydrocarbons, reservoir bitumen, or tar[6]) are brown to black almost solid substances. They are known for their complex structure. Dissolve only in aromatic solvents such as benzene or toluene. Commonly they are known as the heaviest and most polar fraction of crude oil (which also contribute to the highest boiling point from all of the crude oil's components). [7]

They do not have a single, unique structure or specific molecular weight. The composition of asphaltenes and the amount of them depends on the hydrocarbon precipitant (occurrence of natural precipitants in the crude oil such as n-heptane), the precipitant-to-oil volumetric ratio, the contact time (time for precipitant to penetrate the micelle), and temperature at which the precipitation occurs.

Asphaltenes consist of condensed aromatic nuclei that have alkyl groups and alicyclic systems. In addition, they frequently possess functional groups with a heteroatom. The fused-ring systems (unit-sheets) are connected via alkyl chains and heteroatom bridges. The atomic ratio of hydrogen to carbon varies between 1 and 1.3. Apart from those two basic elements, one can frequently find other elements such as sulphur, oxygen, nitrogen, and metals (the most common ones are nickel, vanadium, and iron). The presence of different functional groups is strongly influencing their physical and chemical properties.[7]

Due to its complex structure, it tends to define asphaltenes not based on chemical classification, but based on their solubility and polarity features.[8] Figure 1[9] presents such classification based on polarity. Since in this work we have only one sample to work with, we are not going to dig into its structure.

Internal

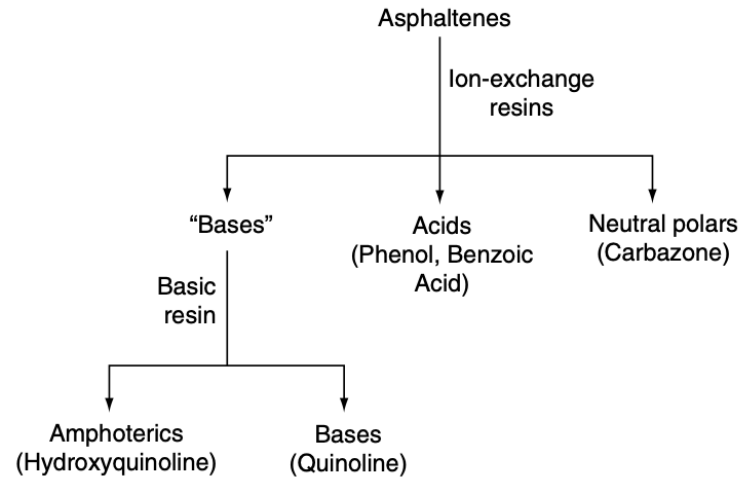

Figure 1 - Asphaltene classification based on polarity [9]

Precipitation of asphaltenes occurs not only due to low temperature but also due to pressure changes. It may occur in the reservoir, production wells, pipelines, or processing plants resulting in severe production problems.

1.1.3 Carbon Dioxide

Carbon dioxide (CO_2) is a stable, non-toxic chemical compound existing as a gas at standard conditions. In petroleum is used either as a gas or as a liquid-like supercritical fluid. When mixed with water, it forms carbonic acid. Carbonic acid tends to be a significant problem for steel elements in the production/injection lines and might cause clogging in carbonate reservoirs.[10] In terms of this work, we are interested in the interaction of carbon dioxide with oil. *Figure 2* [10] presents the solubility of the gas in a dead stock tank oil (where UOP - Universal oil products characterization factor: factor based on boiling point and specific gravity of the oil) concerning temperature and pressure. From this chart, we can see that the solubility increases with rising pressure and temperature.

As mentioned before, CO2 is usually injected as a gas or as a liquid-like supercritical fluid (substance above its critical temperature having properties not usually found at ambient conditions[9]) The fluid density in reservoir conditions is the main factor that determines minimum miscibility pressure (MMP) of CO2 (MMP described in next section) with reservoirs oils[10]. From *Figure 3 - CO2 phase diagram [10]* is observed that the supercritical state of the fluid can be achieved above 80 atm (bar) / 50°C.

Internal

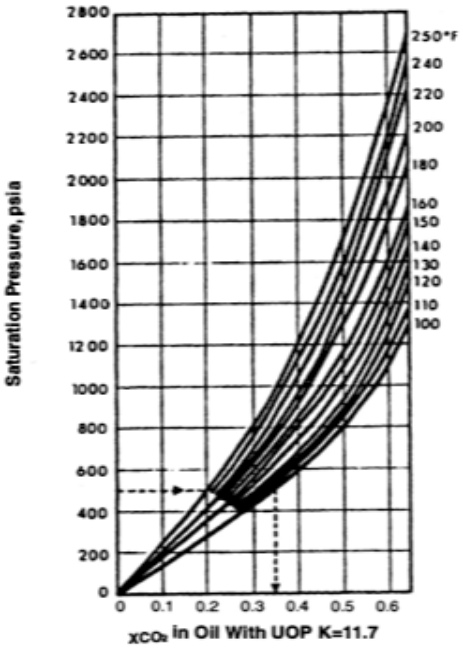

Figure 2 - CO2 solubility in stock tank oil [10]

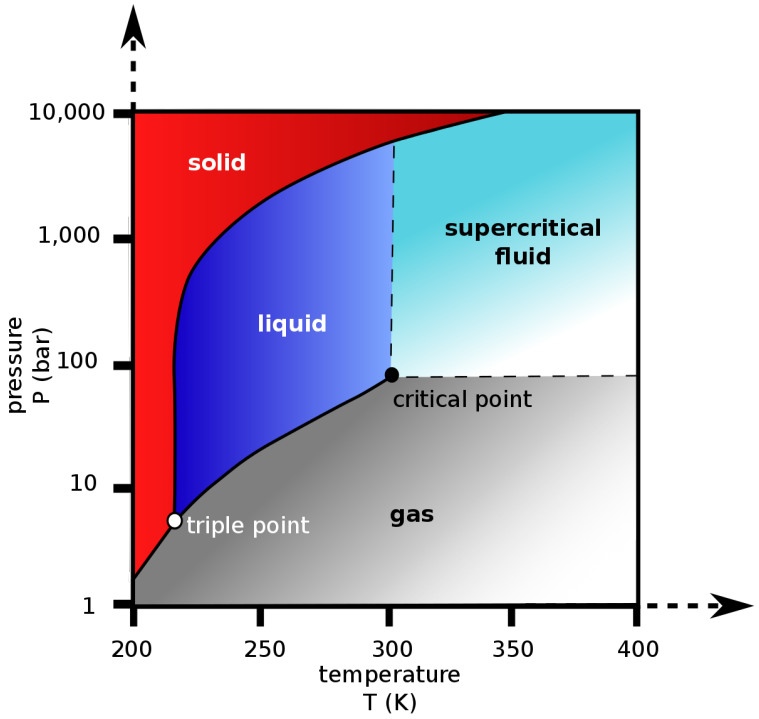

Figure 3 - CO2 phase diagram [10]

1.2 CO_2 flooding mechanisms

1.2.1 Immiscible CO2 flooding

One of the mechanisms regarding CO2 injection is immiscible flooding of carbon dioxide. This method is successful when it comes to viscous, heavy-oil reservoirs. The presence of the agent is contributing to oil swelling and reduction of oil viscosity, which further leads to improved sweep efficiency. The best reservoirs for this type of flooding are low-pressure reservoirs with stock-tank oil gravities less than around 30° API[10].

1.2.2 Miscible CO2 flooding

The most common mechanism during CO2 injection is miscible flooding. The gas after reaching the reservoir mixes with the fluids and influences oil-gas equilibrium. Shifts in equilibrium may affect the phases, thus changing the behavior of the fluid in the system. There are three possible scenarios in this case[11]:

- Vaporizing mechanism – gas takes up components from the oil phase
- Condensing mechanism – oil takes up components from the gas phase
- Combined vaporizing/condensing mechanism – both oil and gas takes up components from each other

The most important factor regarding miscibility flooding is minimum miscibility pressure (MMP). It is the lowest pressure (at fixed temperature) at which miscibility can be achieved between reservoir fluid and injection gas. The lowest pressure at which this can be achieved is called First contact minimum miscibility pressure[11].

Internal

1.3 Laboratory PVT tests

1.3.1 Single flash test (Separator test)

Single flash test (sometimes known as separator test) is a basic pressure, volume, temperature(PVT) experiment that can help identify compositional and volumetric changes that the fluid will undergo during production. The pressurized oil sample is placed in a closed-cell under a given temperature and pressure in which it exists in two phases. The separator test usually follows the constant mass expansion test, using the same sample that has reached a two-phase region but is still above standard conditions. Separator tests can be run in multiple stages, by setting specific pressure ranges (for example mimic separation process at the production site). After equilibrium between two phases is reached, the gas is pumped out of the cell through a gas meter so the volume can be recorded and the gas-oil ratio (GOR) calculated after. The experiment is carried out until the standard conditions are reached. Then while having two containers (one with stock tank oil and one with gas) the other important parameters of fluids in standard conditions can be measured such as volume (V_o -oil volume, V_g–gas volume), density(ρ_o – oil density), the molecular weight of oil(M_o) and composition (x_i – mole ratio of oil component i, y_i – mole ratio of gas component). [11]. Figure 4 - Single flash schematic illustration for bottom hole sample (BHS) testing presents schematic illustration for the single flash test [11].

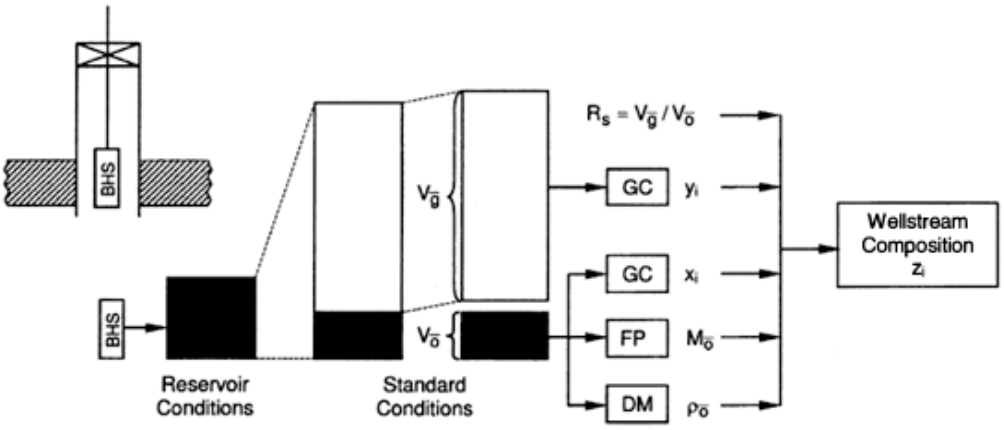

Figure 4 - Single flash schematic illustration for bottom hole sample (BHS) testing [11]

1.3.2 Composition analysis

Gas and oil compositions are obtained by using the gas chromatography technique. Typical Gas Chromatograph consists of an injector, a column, and a detector (basic sketch is presented in Figure 5) [11]

A fluid subsample (gas or liquid) is injected into the column through the injector equipped with a valve system (when gas is injected) or with a syringe (for liquid samples). For gas samples, there is a total of three columns through which carrier gas is constantly moving the sample to keep the separation of the components. Each of those columns has different

Internal

packing. One is packed with porous polymer, the other one with a molecular sieve, and the last one is a capillary column made of fused silica that is bonded with a liquid phase. The reason for having three columns is that they can provide clear identification of all eluted components. For fluid samples, only the capillary column is used. After each component has been successfully separated, the carrier gas flows into the detector. It produces an electrical signal proportional to the amount of the component in the sample. When it comes to liquid samples there is a flame ionization detector mounted, whereas for gas samples there is additionally thermal conductivity detector used together with the other detector. Since each of the components is freed at a certain temperature, the whole system is placed in an enclosed temperature-controlled environment [11].

Obtained data provide the weight percentage composition of each hydrocarbon. The standard analysis includes the distinguishment between iso and normal C_4 and C_5 hydrocarbons. The more advanced gas chromatographs can offer detailed composition even up to C_9. The rest of the more heavy components are grouped into carbon number fractions according to the boiling ranges.

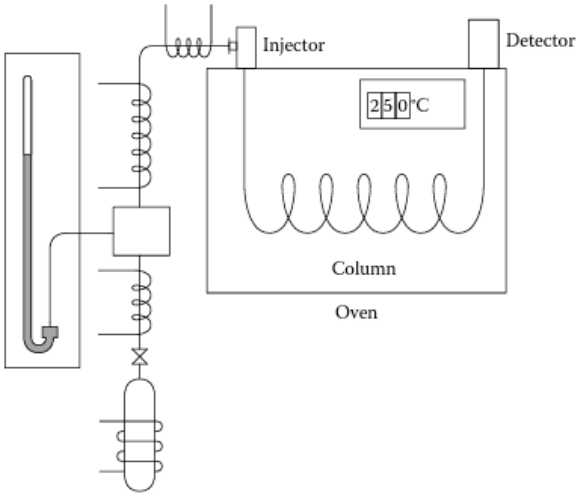

Figure 5 - Sketch of the Gas chromatograph [5]

1.3.3 Constant mass expansion

Constant mass expansion (also known as Constant composition expansion or pressure-volume test[11]) is a laboratory test performed to find basic pressure-volume relation data such as the bubble-point the pressure, the undersaturated oil density, the iso-thermal oil compressibility, and the two-phase volumetric behaviour at a pressure below the bubble-point pressure[10].

The pressurized fluid sample is transferred at a given temperature (usually slightly above reservoir) and given pressure (usually above the reservoir pressure, to make sure the sample exists in one phase) to a cell, equipped with the piston at one end. The cell is also equipped with a thermostat and stirrer to keep the temperature constant throughout the test and

Internal

to properly mix the fluid. After waiting for the sample to stabilize in the cell, the initial volume of fluid is measured and a constant mass expansion experiment can start. The volume of the cell is increased by adjusting the piston, which causes the pressure to decrease. At predefined pressure steps, the sample is left to stabilize again and the volume is noted. Usually, each pressure step is from 10-25 bar. The process is repeated until the abandonment pressure is reached (for example separator pressure). The pressure point at which fluid enters the two-phase region (saturation point) is the bubble point [11]. This is assessed based on relative volume V_{rel} (equation 1) It is the ratio of recorded total volume V_{Tot} to volume at saturation pressure V_{sat}. For $V_{rel} = 1$ we have reached saturation pressure. A schematic illustration of the process is presented in Figure 6 - Constant mass expansion for oil mixture [11]. We can observe how piston-powered with water is used to change the pressure in the sample side of the cell. The scheme illustrates 5 important steps of the process and how it influences the phase behavior of the sample (from left to right): Pressure in the cell way above bubble point pressure(1 phase), pressure in the cell above bubble point pressure (1 phase), pressure in the cell equal to the bubble point (1 phase), pressure in the cell below bubble point pressure (2 phases), pressure in the cell way below bubble point pressure (2 phase)

$$V_{rel} = \frac{V_{tot}}{V_{sat}} \qquad \textit{Eq. 1}$$

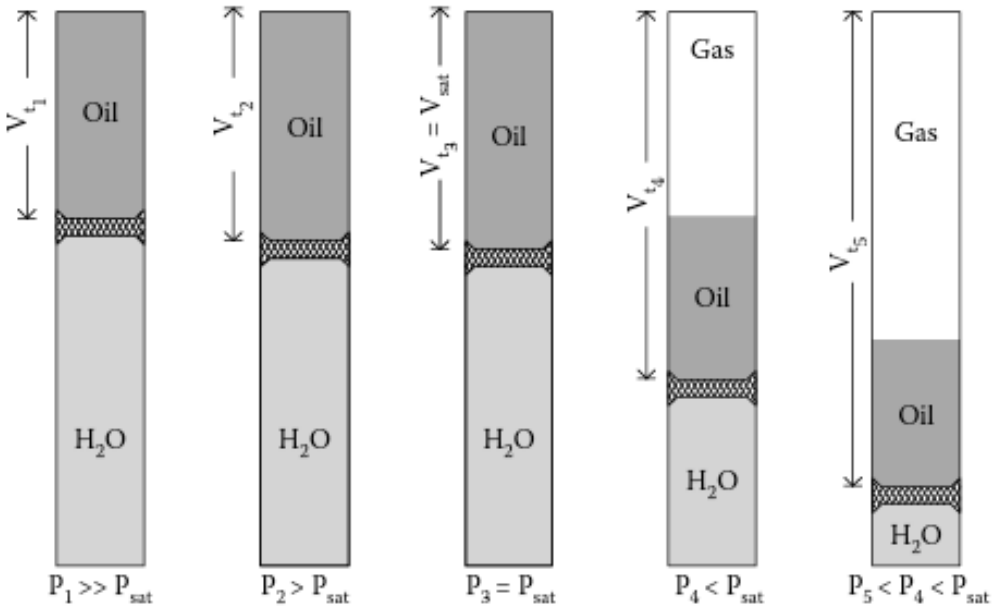

Figure 6 - Constant mass expansion for oil mixture [11]

1.3.4 Density measurement

The density of stock tank oil is measured with a digital density meter (designed by Anton Parr). They are based on the oscillating U-tube principle. The U-shaped glass tube is excited which produces oscillation at a certain frequency depending on the sample type being measured. By measuring the frequency of vibration, the fluid density can be calculated. Those are very effective and fast machines that can give precise measurements of the density (accuracy up to 0,0002 g/cm^3).[12].

Internal

1.3.5 Titration test

At each step certain, known mole amount of injection gas is added to the sample in the Vinci cell under constant pressure. At each step, after injecting the gas, the sample is left for some time to mix and stabilize and light transmittance is read. The test is run until there is clear light transmittance disturbance caused by entering the two-phase region. This experiment gives a better understanding of how the injection fluid is influencing the saturation pressure. At each step the pressure, temperature, and volume must be obtained, both in the cell and in the injection gas bottle, so the exact amount of moles can be calculated. This is done as following [13]:

- Mole ratio of gas added (%mol):

$$\%mol = \frac{n_g}{n_o} \quad \textit{Eq. 2}$$

- Mole number of gas (n_g)

$$n_g = \frac{z \cdot R \cdot T}{P \cdot v} \quad \textit{Eq. 3}$$

- Compressibility factor (z)
  Calculation of 'z' factor is based on iterative Newton-Raphson method, based on Soave-Redlich-Kwong equation of the state transformation. The compressibility factor is pressure and temperature dependant, hence it is crucial to calculate it at each step of injection. A detailed solution for solving the equation is presented in the appendix.

$$z^3 - z^2 + (A - B + B^2) \cdot z - AB = 0 \quad \textit{Eq. 4}$$

1.4 Asphaltene experiments

1.4.1 Near infra-red light scattering for the asphaltene onset pressure measurements

The light scattering technique is the most common technique for the detection of asphaltene onset pressure (Pressure at which asphaltenes start to precipitate from the oil). The experiment is about measuring near-infrared light transmittance in the oil. The fluid sample is transferred to the pressurized and heated cell (equipped with a piston to control pressure). The cell has a light source on one side and a receiver on the other one (*Figure 8).* The cell is gradually depressurized. When pressure is above upper asphaltene onset pressure (upper AOP), the fluid is homogenous and there are no suspended solids, so the lights travel through the sample basically without any scattering. While reaching and surpassing the upper AOP, asphaltenes start to precipitate and the light is partially scattered. The light's transmittance is gradually decreasing, as more and more asphaltenes appear with decreasing pressure in the cell. Until the bubble point being reached, then total scattering takes place. When approaching lower AOP the light transmittance starts to rise again as light components are dissolving asphaltenes. This process is presented in *Figure 7* [11].

Internal

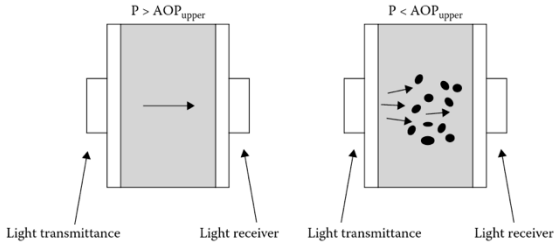

Figure 8 - Light scattering technique [11]

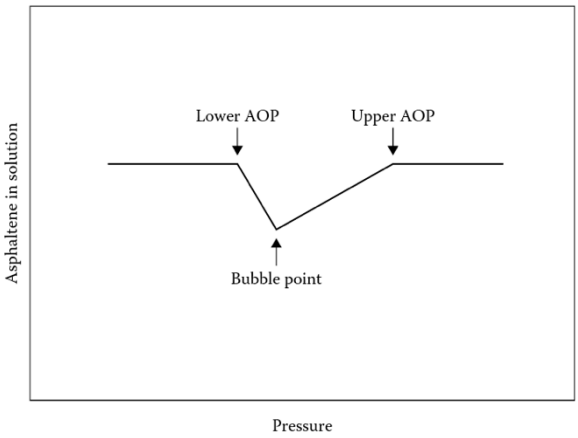

Figure 7 - Asphaltene content - pressure relation [11]

1.4.2 SARA analysis

For detailed content of not only asphaltenes but also saturates, aromatics, and resins (SARA), the SARA analysis is carried out.

"Moreoil" method is carried out that follows NIGGOGA, 4th edition procedures. Around 5g of oil is weighed. Then around 200g of n-pentane is added (volume ration 1:40). The solution is mixed in the ultrasonic bath for 15 minutes and then stored dark at room temperature for a minimum of 24 hours. Then the solution is filtered with a filtration unit connected to a water jet pump. Filter pore size 0,45 μm. After the process is finished cake on the paper is washed with n-pentane. The filter with asphaltenes is put at 100°C for 30 min, then transferred to a desiccator and cooled to constant weight. Then weight ratio of asphaltenes to oil weight can be calculated.

Due to the lack of equipment in our lab, the measurement was carried out by 3rd part company.

1.5 Apparatus

For Constant Mass Expansion tests and Asphaltene onset, pressure measurement PVT cell produced by Vinci Technologies was used. The cell enables hydrocarbon phase behavior studies at reservoir conditions. Equipped with an embedded high-pressure pump that serves as a controlling and monitoring mechanism for fluid pressure and volume in the cell. Magnetically coupled stirrer provides fast thermos-physical equilibrium and proper mixing of the sample. The cell is fixed in the air-bath that is ensuring stable temperature throughout the measurement.

Build-in macros enable a fully automatic process. By setting pressure steps for depressurization, stabilization time for taking the reading, and end pressure point, we were able to ensure smooth and reliable measurement that in some cases took even 48 hours. The output

Internal

consisted of recorded volume and light transmittance at the previously defined pressure step. [14]

The cell is also equipped with a solid detection system (SDS). This instrument is designed to detect any organic deposition occurring in the sample. It measures low-intensity laser light transmittance through fiber optic transmission probes mounted across a windowed cell. The instrument consists of a light source that generates the signal penetrating fluid, a power meter to measure the attenuated signal, two fiber optic transmission probes, and a data acquisition software used to record system pressure, temperature, solvent flow rate, and the power of the transmitted light.[15]

1.6 PVT modeling

1.6.1 Equations of State

Every fluid can be represented by cubic equations of state (EOS) which can accurately relate pressure, volume, and temperature relations. With known fluid composition and each of the component's critical properties and acentric factors, one can easily describe volumetric and phase behavior. The prior can be calculated by solving a simple cubic equation that has its origin in ideal gas law:

$$z = \frac{p \cdot v}{RT} \qquad \textit{Eq. 5}$$

Which is usually presented in the form of:

$$z^3 + A_2 \cdot z^2 + A_1 \cdot z + A_0 = 0 \qquad \textit{Eq. 6}$$

Where A_2, A_1, and A_0 are functions of pressure, temperature, and composition.

Phase equilibria need to be calculated with Equations of the state by satisfying chemical equilibrium. Chemical potential(μ_i) of each of the components in the liquid phase must equal one of each component in the vapour phase. It is expressed as fugacity (f_i) [10].

The pioneer equation was the one introduced in 1873 by Van der Waals. Since then, a lot more equations have been proposed, but most of them kept the original form of the one introduced by Van der Waals. One of the most popular in the industry now is Soave-Redlich-Kwong-Peneloux. [11]

$$P = \frac{RT}{V-b} - \frac{a(T)}{(V+c)(V+b+2c)} \qquad \textit{Eq. 7}$$

Where:

$$a(T) = a_c \cdot \alpha(T) \qquad \textit{Eq. 8}$$

Internal

$$a_c = \frac{0.42747 R^2 T_c^2}{P_c} \quad \text{Eq. 9}$$

$$b = \frac{0.08664 R T_c}{P_c} \quad \text{Eq. 10}$$

$$\alpha(T) = (1 + m\left(1 - \sqrt{\frac{T}{T_c}}\right))^2 \quad \text{Eq. 11}$$

$$m = 0.480 + 1.574\omega - 0.176\omega^2 \quad \text{Eq. 12}$$

$$c = \frac{0.40768\, R \cdot T_c \cdot (0.29441 - Z_{RA})}{P_c} \quad \text{Eq. 13}$$

$$Z_{RA} = 0.29056 - 0.08775\omega \quad \text{Eq. 14}$$

The equation incorporates each of the component's properties like critical temperature (T_c), critical pressure (P_c), and acentric factor (ω). For multi-component mixture, Soave introduced a new way to calculate parameters ***a*** and ***b***. This method introduces Binary interaction coefficients *k* (BIC) between two components *i* and *j*. For two of the same compounds, k_{ij} is equal to 0. When we consider two different nonpolar components, BIC will be equal or close to zero. When it comes to binary pairs where one of them is polar, k_{ij} will be nonzero. The equations for *a* and *b* including binary interaction coefficients looks like: [11]

$$a = \sum_{i=1}^{N} x_i \cdot x_j \cdot a_{ij} \quad \text{Eq. 15}$$

$$b = \sum_{i=1}^{N} x_i \cdot b_i \quad \text{Eq. 16}$$

$$a_{ij} = \sqrt{a_i \cdot a_j} \cdot (1 - k_{ij}) \quad \text{Eq. 17}$$

1.6.2 Tunning

As mentioned earlier, oil is a complex mixture of multiple hydrocarbons where some of them have an extremally high carbon number. To simplify calculations it is common practice to lump heavy components into a grouped pseudo-components. Such lumping however often deteriorates the quality of PVT simulation, as properties of lumped compounds are averaged.[11]

To make up for those differences, a common practice is the tunning of the component's properties. This is done by regression on object function. In PVT tunning it is minimizing the objective function. Since linear regression is a complex topic it is not detailed in this work.

The most uncertain parameters in the fluid (the parameters mostly changed during regression) are properties of the heavy pseudo-components. The biggest points of interest are critical pressures and temperatures, molar weights, acentric factors, and BIC between light components and injected gas (In our case CO_2).

Internal

1.6.3 Asphaltene modelling

Asphaltene modelling module in the PVTsim is calculating asphaltene precipitation using the equation of the state. By default, any aromatic fraction C_{50+} is considered to be asphaltene. However, by inserting the experimental value of asphaltene content based on SARA analysis, the user can tune the cut point adequately. When pseudo-component is considered to contain asphaltenes, it is split into an asphaltene and non-asphaltene component with different properties for each of them. Unfortunately, the software developer does not precisely describe the exact workflow for the calculations of precipitation.

Samples

1.7 Available samples

Originally we started with two pressurized samples from one of the operators producing on the North Continental Shelf. Both of them were supposed to be bottom hole samples (BHS), but after closer examination one of them turned out to be a pressurized separator sample, sampled at P = 6 bar. Low sampling pressure and potential lack of light components brought doubts about asphaltene content and value for future asphaltene precipitation studies. The other sample according to the datasheet was supposed to be BHS, but the bottle in which the sample was stored turned out to have a damaged valve, making it impossible to extract its content.

Due to the given circumstances and after reviewing the test run on the separator sample (that will be described later in the work), we have decided to recombine this sample with certain rich gas to create an artificial bottom hole sample and increase its bubble point pressure.

1.8 Sample storage

Pressurized oil samples are stored in special titanium bottles (cylinders). The bottle is equipped with two valves, one on each side. The inside of the bottle is divided into two parts by a floating piston. The position of the piston can be adjusted by injecting glycol-water mixture through one side of the bottle and the corresponding valve (water side). This mechanism enables to adjust of the pressure of the sample on the other side of the piston (sample side). Inside of the sample side, there is also a steel ball. The presence of the ball is crucial in terms of mixing the sample. By rotating the bottle, the ball moves freely through the sample, introducing mixing. Figure 9 presents a photo of such a cylinder. [16]

Internal

Figure 9 - Pressurized sample bottle (cylinder) [16]

1.9 Sample conditioning, cell preparation, and sample transferring procedure

As mentioned earlier, asphaltene precipitation occurs due to a drop in pressure and temperature. To make sure all the asphaltenes have been redissolved in the fluid, before each measurement which required taking some sample out of the bottle, it was placed in a heating jacket and put on mixing for 2-3 days. Before that sample has been pressurized to 400 bar, which is pressure way above bubble point to make sure the sample stays in 1 phase.

For most of our work here we have used Vinci cell. Before each of the measurements (AOP, CME, or Titration) the cell and the heated transferring line have been vacuumed to minimize the presence of air or other gases that could disturb instruments reading. Next, the sample was transferred with slow and steady valve openings to avoid huge pressure drops, potentially leading to a two-phase state. To the water side of the bottle, a volumetric pump was connected to make up for any pressure losses and maintain steady pressure in the sample cylinder. Once the cell has been filled up with the necessary volume of sample (around 35 cm^3), it has been left for at least 24 hours to stabilize in the cell with the mixer turned on. The indicator for a stable sample was a steady light transmittance signal recorded with SDS equipment. High variance in signal indicates instability of the sample (as presented in

Figure 10), whereas rather a low variance indicates that the sample is stable and ready for the start of measurement (

Figure 11).

Internal

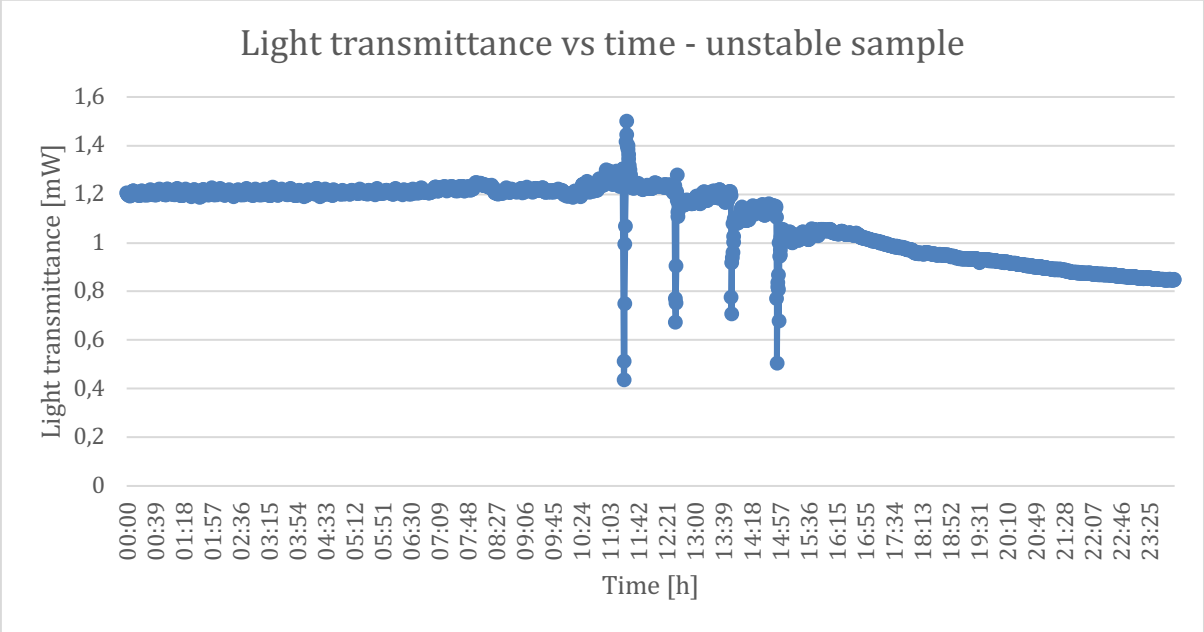

Figure 10 – unstable sample example

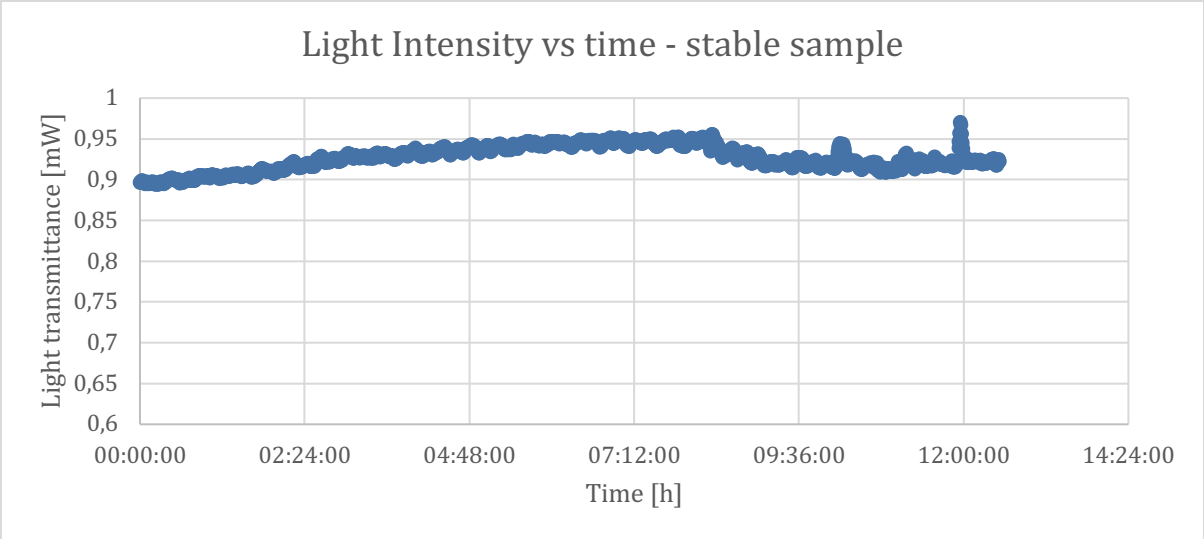

Figure 11 - stable sample example

After every measurement, the cell has been washed under pressure with solvents. First three times with toluene and then at least three times with hexane to ensure neat cell for next tests.

Internal

Experiments

1.10 Separator sample

1.10.1 Constant mass expansion and asphaltene onset pressure

To better understand the sample we have received, asphaltene onset pressure measurement combined with constant mass expansion was run. This gave us an understanding of bubble point pressure and asphaltene appearance. Also, this was the first step of sample preparation for the next measurements such as single flash, composition analysis, and SARA analysis.

Following the procedure mentioned in paragraph 4.3, around 35 cm^3 of the sample was transferred to the cell via a heated line. After stabilization, the macro was run to perform gradual depressurization. Results are presented in Table 1 and plotted on Figure 12 - CME & AOP measurement for separator sample

Internal

Pressure	Total Cell Volume	SDS Power
(bara)	(cc)	(W)
475	39,835	8,222E-04
450	39,868	8,082E-04
425	39,904	7,890E-04
400	39,941	7,838E-04
375	39,981	7,717E-04
350	40,024	7,738E-04
325	40,068	7,795E-04
300	40,114	7,794E-04
275	40,163	7,825E-04
250	40,214	7,839E-04
240	40,235	7,856E-04
230	40,257	7,837E-04
220	40,278	7,834E-04
210	40,301	7,818E-04
200	40,319	7,745E-04
190	40,336	7,690E-04
180	40,339	7,648E-04
170	40,371	7,604E-04
160	40,4	7,608E-04
150	40,427	7,672E-04
140	40,456	7,757E-04
130	40,485	7,763E-04
120	40,514	7,835E-04
110	40,544	7,779E-04
100	40,574	7,623E-04
90	40,605	7,629E-04
80	40,635	7,623E-04
70	40,669	7,627E-04
60	40,703	7,676E-04
50	40,738	7,743E-04
40	40,779	7,812E-04
10	40,973	7,695E-04
8	41,021	7,417E-04
6	41,09	7,302E-04
4	42,077	6,182E-04
2,3	61,675	6,135E-04
1,9	74,808	6,020E-04

Table 1- CME & AOP measurement for separator sample

Internal

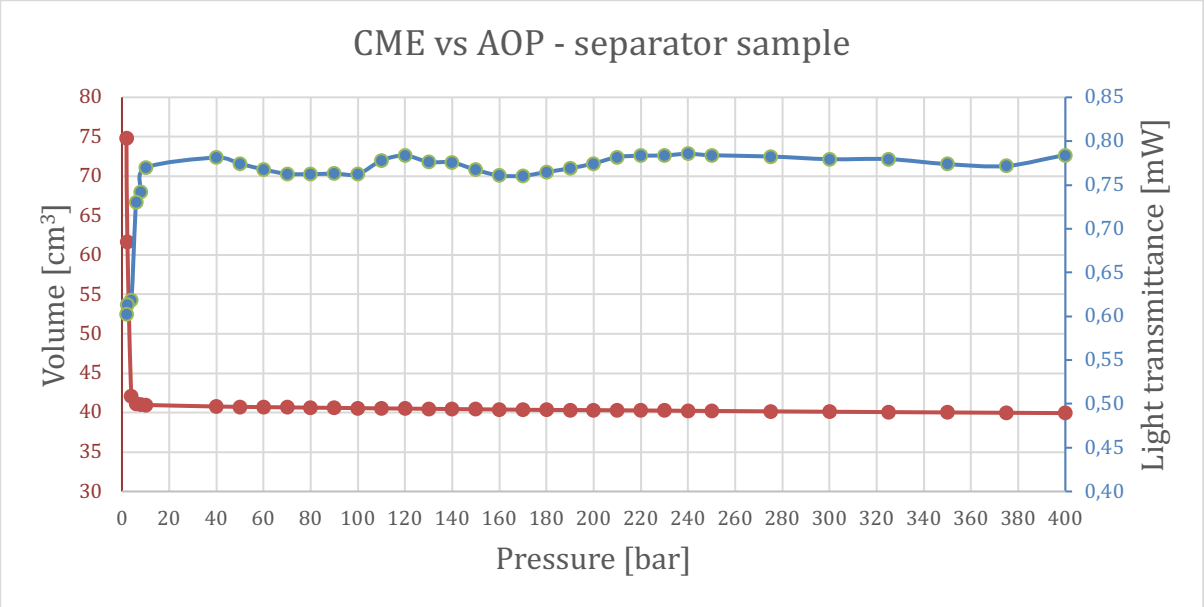

Figure 12 - CME & AOP measurement for separator sample

From the results, we can clearly see that due to the fact, that the oil sample was taken from the separator at 6 bar, there is a lack of light components resulting in low bubble-point pressure (around 6 bar). Light transmittance did not indicate any trends, which put in doubt whether it will be possible to work on the asphaltene precipitation with this sample. Nevertheless, we have decided that we are going to perform couple more tests, including SARA analysis to decide about the future of that sample.

1.10.2 Single flash and density measurement

After the previous measurement, the sample has been slightly pressurized inside the cell (using cell piston) and then a small subsample has been transferred under pressure to the container (Mass of the empty container has been previously measured with digital scale). Then, the mass of the container with the sample has been measured. The next step was to connect the container to the gasometer, and by slow depressurization, separate gas, and oil. Volume and pressure of separated gas have been recorded and gas has been transferred to an earlier connected special container. The container with residual oil, after establishing ambient pressure, has been disconnected and the mass of the container with dead stock tank oil has been measured. Three subsamples of stock tank oil have been taken, one each for the following measurements: Density of stock tank oil (STO), Composition analysis, and SARA analysis. Separated gas has been preserved for the following studies: Gas composition and gas density. Empty container for gas storage has also been weighted, and after filling it with gas, mass was measured again.

Once the density of the stock tank oil has been measured, as described in 1.3.4 and the mass of the stock tank oil has been calculated (By subtracting the mass of the empty container from the mass of the container filled with stock tank oil), the volume of stock tank oil could be calculated. Once this has been found, the gas-oil ratio for the sample could be calculated. All of the results from the measurements described above are presented in Table 2.

Internal

Gas-oil ratio (GOR)	7,8	Sm^3/Sm^3
Oil formation volume factor at separation pressure	1,030	m^3/Sm^3
Oil formation volume factor at saturation pressure	0,922	m^3/Sm^3
Density of stock tank oil	845,2	kg/Sm^3
Density of oil at P_{BP}	933,3	kg/m^3
Gas gravity:	1,638	-

Table 2 - Single flash and density measurement

1.10.3 Composition analysis

The next step in the work was to establish what is the sample made of. Those measurements were carried out by the specialized staff of the Stratum reservoir chromatography lab. The overview of fluid composition is presented in Figure 13 with respect to oil and gas and also calculated total fluid composition. The detailed composition has been presented in appendix 1.22. Oil is rich in heavy components that make up more than 50% of the total composition. Propane and butane are the main components of the gas. A low amount of methane and ethane seems reasonable since the fluid was sampled at 6 bar where most of the light components have already been stripped off the fluid.

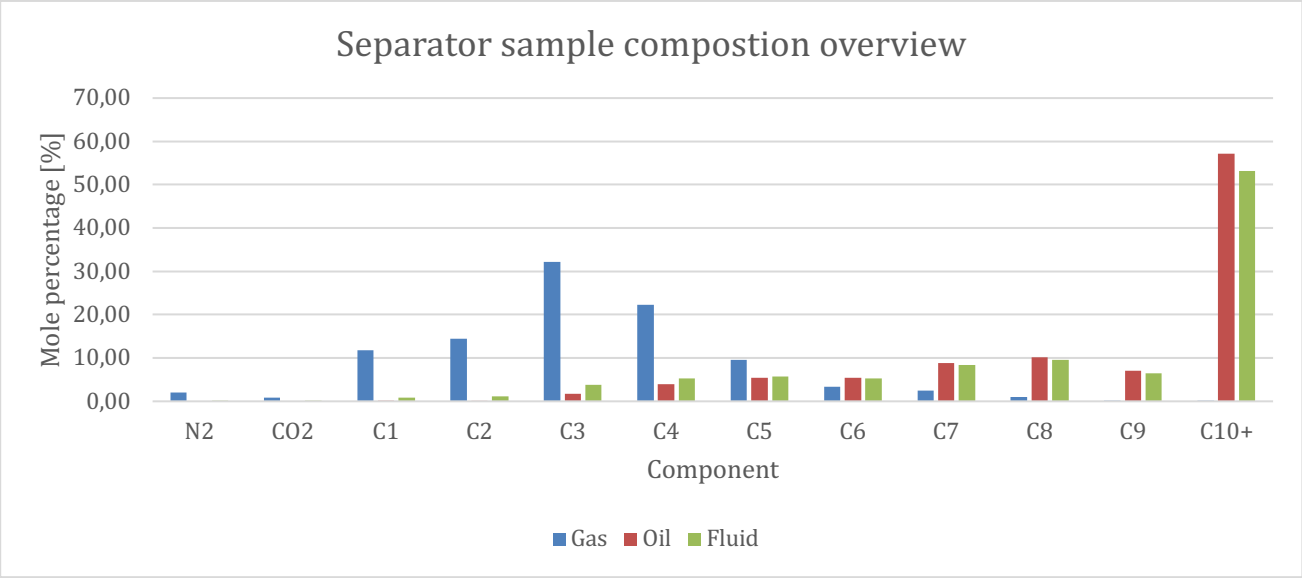

Figure 13 - Separator sample composition overview

Internal

1.10.4 SARA analysis

The final test that was about to indicate whether or not the sample contains any asphaltenes was SARA analysis. As mentioned earlier, due to lack of equipment to conduct such test, stock tank oil sample has been sent to 3rd party company. Table 3 presents the result. Asphaltene content has been assessed at almost 1% of the sample.

Component	Saturates	Aromatics	Resins	Asphaltenes
Weight percentage [%]	59,3	31	8,9	0,9
Hydrocarbons share [weight percentage %]: 90,2				

Table 3 - SARA analysis

1.10.5 Conclusions

After careful analysis of the gathered data and potential for asphaltene study, we have decided to continue working with this sample, but with some adjustments. Since the beginning, we have planned to work with a bottom-hole sample that could provide us with full, untouched reservoir fluid. Such fluid would be more relevant in terms of studying asphaltene precipitation during CO_2 injection in the reservoir, which takes place in high pressure, high temperature, and with unchanged oil and gas composition. To be as close to such conditions as possible, we have decided to recombine the separator sample with rich gas (high methane content) and proceed with CO_2 studies on that sample.

1.11 Recombined sample - basic PVT measurements

1.11.1 Constant mass expansion (run simultaneously with AOP)

Once the new sample was created (By recombination), the first step was to assess bubble-point pressure. It was a crucial point, as bubble-point pressure was indicating what is the minimum pressure we can bring pressure in the sample down to while still keeping the sample in one phase. As described earlier, light transmittance can be disturbed either by gas coming out of oil or by asphaltene particles. Knowing what is one phase zone in terms of pressure, we could assume that whenever there is a drop in signal, it was caused by asphaltenes.

Coming back to constant mass expansion. A sudden increment in volume indicates gas releasing from the oil. The data points have been plotted (Figure 14) and two trend lines were created (one corresponding to the one-phase zone and the other one to the two-phase zone). Based on those results we can observe bubble point around 120 bar, that is where the trend lines cross.

Internal

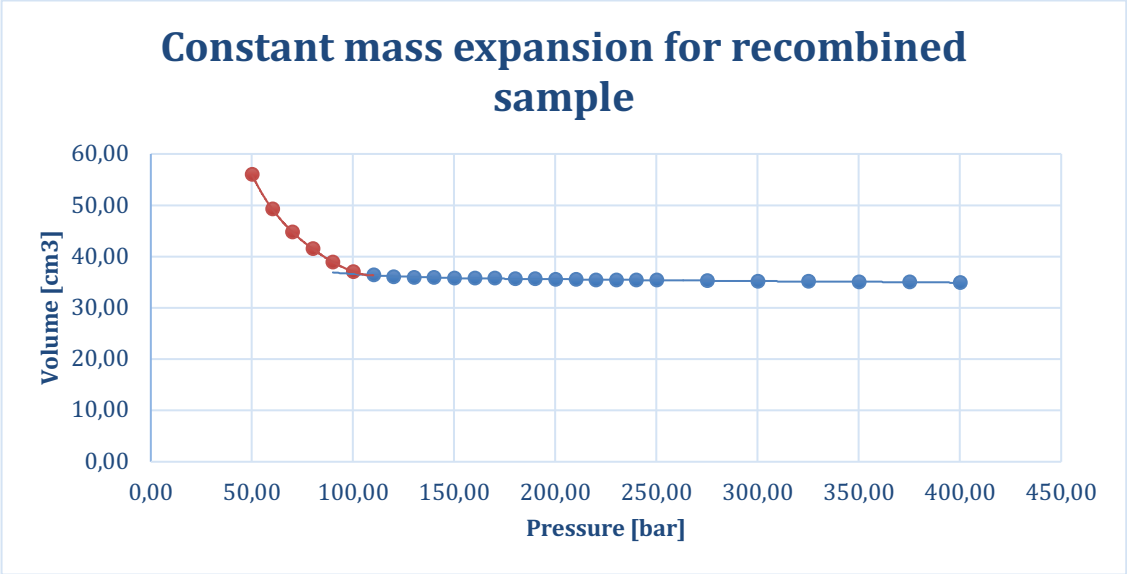

Figure 14 - Constant mass expansion for recombined sample

1.11.2 Single flash and density measurement

Following the same procedure as in 1.10.2, the gas-oil ratio and density have been acquired. Results are presented in Table 4. We can clearly see that by introducing rich gas, GOR has increased more than 10 times. Also, some of the gas components lastingly dissolved in oil, slightly increasing stock tank oil density.

GOR	82,6824	Sm^3/Sm^3
Density of stock tank oil	846,95	kg/Sm^3
Gas gravity	0,95151	-

Table 4 - Single flash and density measurement for the recombined sample

1.11.3 Composition

The next step was to establish the composition of the new fluid. This measurement was conducted again entirely by the experienced Chromatography Lab of Stratum Reservoir. The overview of the results is presented in Figure 15. A detailed composition can be found in Appendix 1.23. Introducing rich gas has decreased the share of heavy components in the fluid from around 60% down to around 32%.

Internal

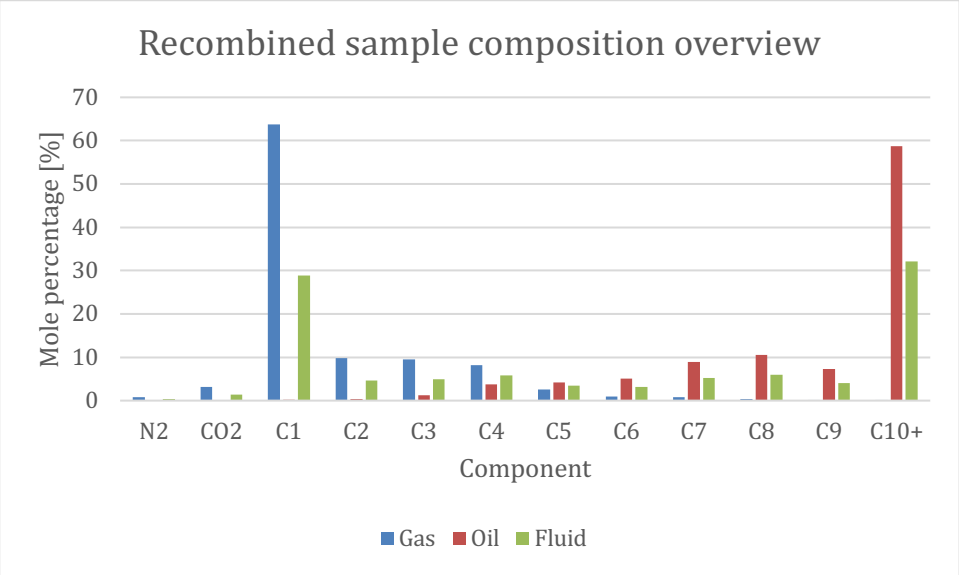

Figure 15 - Recombined sample composition overview

1.12 Recombined sample – Titration

To check how CO_2 is influencing the sample, in this example how the light transmittance is developing under the presence of the injected fluid, a titration test has been conducted. We wanted to confirm our theory that increasing content of carbon dioxide will disturb the system and asphaltene will start to precipitate. This would be indicated by a decline in light transmittance. In our test, we have decided to conduct the measurement in constant pressure 250 bar. After transferring 35,945 cm^3 of sample to Vinci cell, with respect to the procedure mentioned earlier, the gradual addition of CO_2 was performed. Due to slight changes in room temperature, the bottle with CO_2 was exposed to minor changes in pressure. In order to keep the fluid stable during injection, pressure in the cell has been always lowered 4 bars below the pressure in the bottle every time injecting took place. After successful injection, the cell has been pressurized back to 250 bar every time. Then the sample has been left for around 1 hour to stabilize with the mixer turned on. Each injection step has been calculated using PVT equations of state (to find the volume of the gas at current conditions. Equations mentioned in 1.3.5) and then mole ratio was calculated. Figure 16 shows the visual representation of the results and Table 5 presents full data for the test. As seen in the figure, the theory has been confirmed, meaning that the more CO_2 in the system, the more asphaltenes are precipitating. This was a promising result in terms of the next test of asphaltene onset pressure for different CO_2 content.

Internal

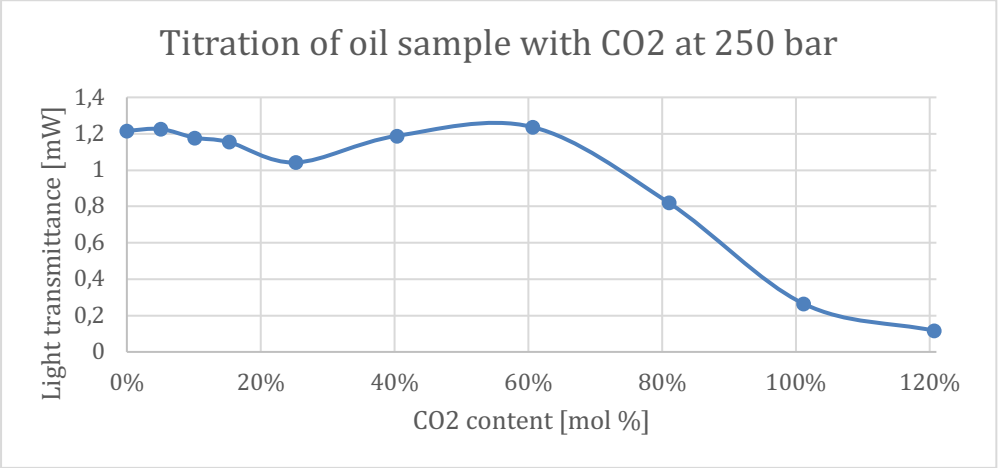

Figure 16 - Titration of oil sample with CO2 at 250 bar

Step	Target mole ratio [%]	P of CO2 bottle [bar]	T in CO2 bottle [°C]	Volume of gas - calculation [cm3]	Volume of gas used [cm3]	Actual mole ratio [%]	Light transmittance [mW]	Comments
0	0	242	21,8	0	0	0,000%	1,216	only sample
1	5	242	21,8	0,508	0,507	5,017%	1,226	
2	10	245	22,3	1,015	1,024	10,129%	1,178	
3	15	249	22,8	1,523	1,542	15,253%	1,154	
4	25	252	23	2,542	2,552	25,260%	1,042	Reading next day
5	40	245	21,6	4,058	4,067	40,321%	1,188	
6	60	253	21,8	6,087	6,096	60,601%	1,237	
7	80	255	22	8,116	8,148	81,015%	0,82	
8	100	256	22,1	10,141	10,167	101,098%	0,266	after 2h reading
9	120	248	22,4	12,166	12,181	120,600%	0,117	

Table 5 - Titration test - full data

Internal

1.13 Recombined sample – AOP measurements

1.13.1 Temperature effect – test in 40°C and 80°C

Before introducing CO_2 to our tests, we wanted to study the temperature effect on asphaltene precipitation. To do so, we have run one AOP test in 40°C. For each of the test runs in the Vinci cell, we had an output that consists of one point that was read after waiting time. Sometimes the results seemed to be misleading, as the reading might fluctuate. Luckily, the software for controlling cell has a logging tool, that takes the reading of pressure, volume, temperature, and light transmittance every half minute (providing almost 4000 measured points). In this measurement, we present both of the plots to show how they can differ, but in the next ones only the more reliable one will be presented. When comparing Figure 17 and Figure 18, we can clearly see that on full log data, the trends are visible, whereas, at the macro output, the trends are misleading. Regarding temperature effect, based on slight decrement in signal for sample in 80°C we have identified the AOP at 140 bar (saturation pressure 120 bar). For the lower temperature sample, there was no clear AOP point, hence we have concluded this measurement to be unreliable.

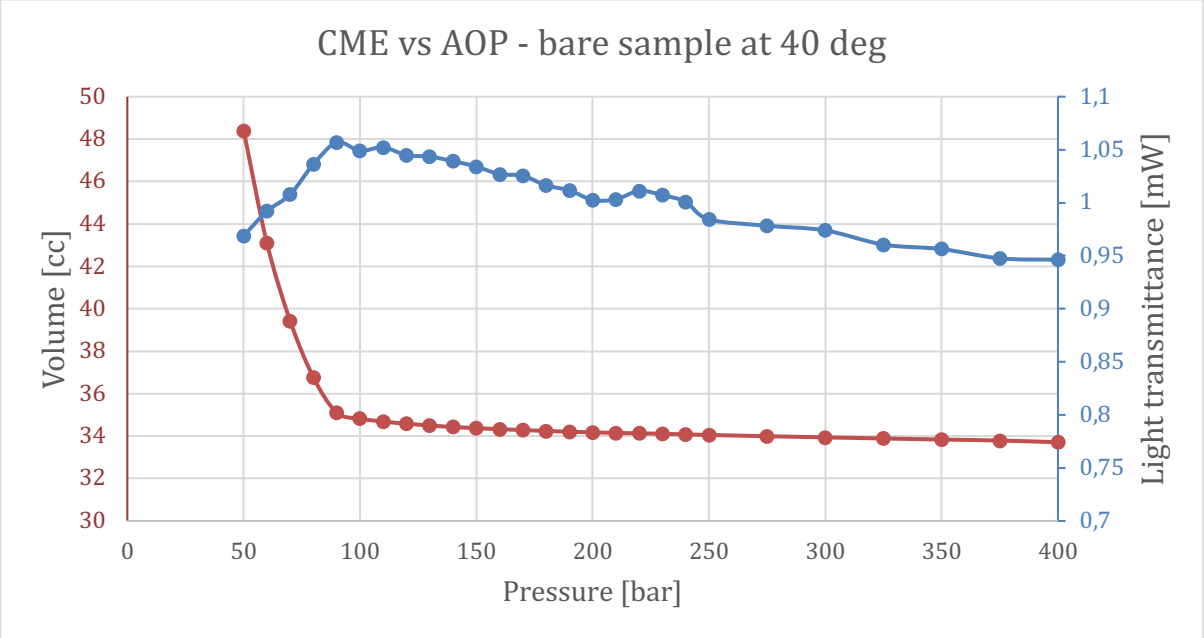

Figure 17 - CME & AOP vs pressure at 40℃, macro output

Internal

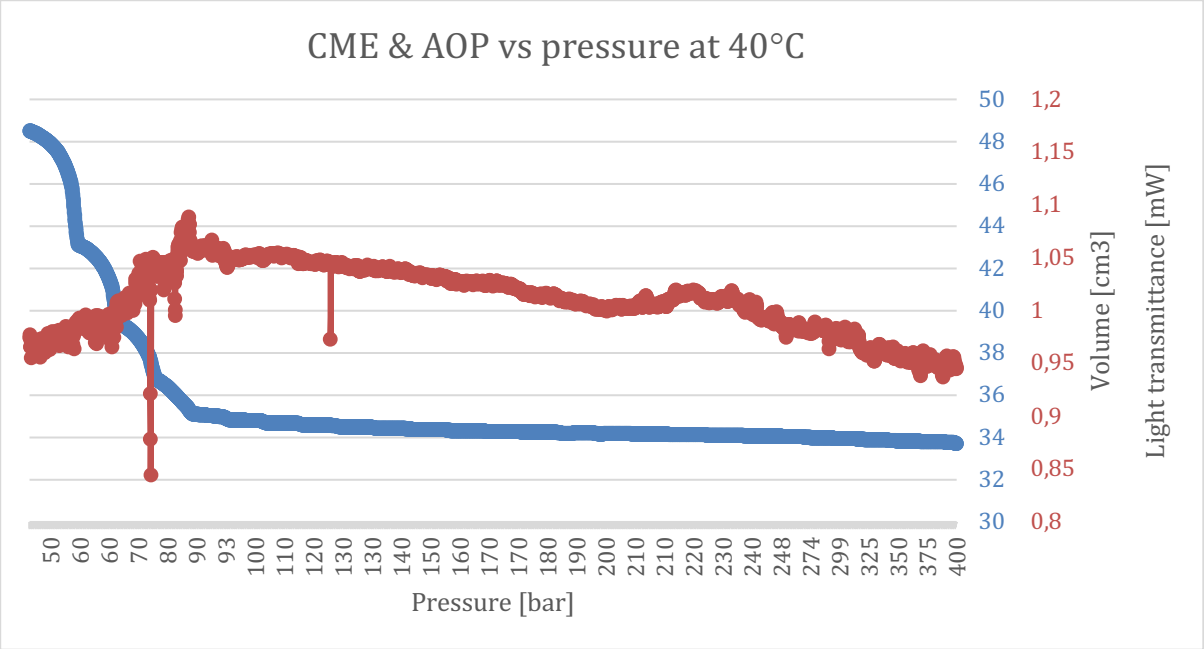

Figure 18 - CME & AOP vs pressure at 40 ℃, full log output

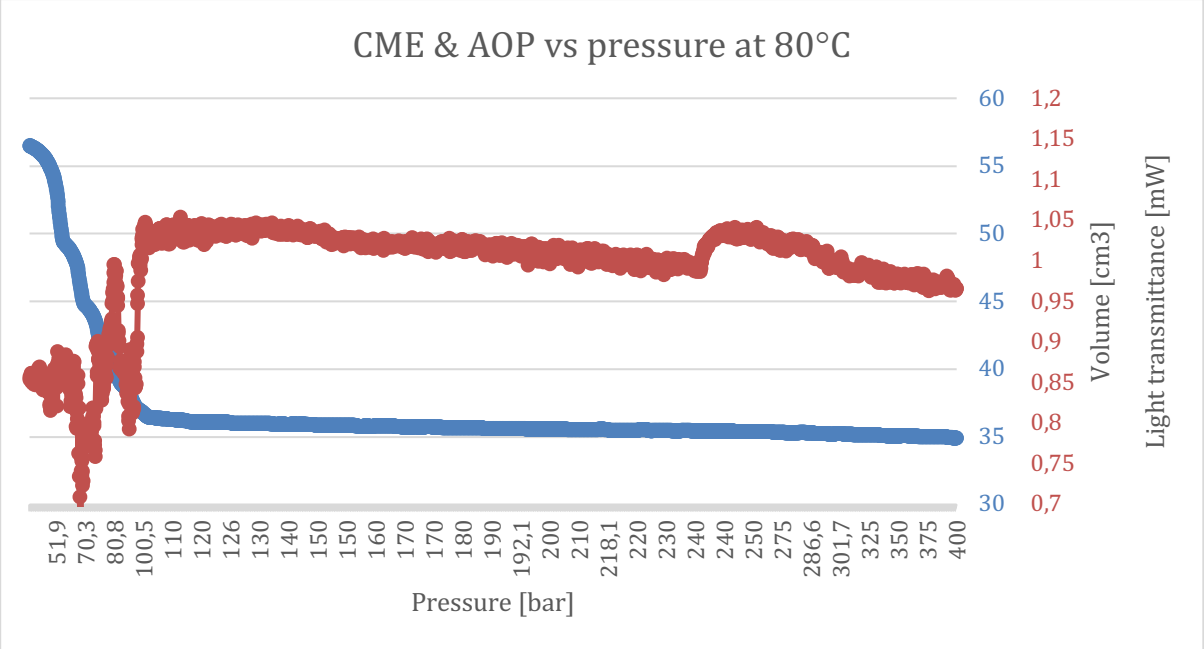

Figure 19 - CME & AOP vs pressure at 80 ℃

Internal

1.13.250 % mole CO_2 added

Next, we wanted to see the effect of carbon dioxide introduced to the live oil sample. Based on the titration experiment we have decided to do 2 tests, each of them with a different CO_2 mole ratio. The first of them was 50 %. The titration test has shown that at this ratio, the sample seemed quite stable in terms of light transmittance (at 250 bar). We studied the full pressure effect for this quantity of gas. After transferring the sample and stabilization time, the next day CO_2 was injected using a precise (± 0,001 cm^3) volumetric pump. The pressure of injection and temperature of the gas bottle was noted, and the precise mole ratio was calculated based on the oil sample in the cell (volume and moles). We ended up with a 50,1% mole content of carbon dioxide. The test was run at 80°C to mimic reservoir conditions. Bubble-point pressure for such composition is proven to be at 180 bar and asphaltene onset pressure appears to be at 220 bar. There is an outline at around 300 bar that breaks the build-up of light transmittance. Adding carbon dioxide, as expected, has increased AOP.

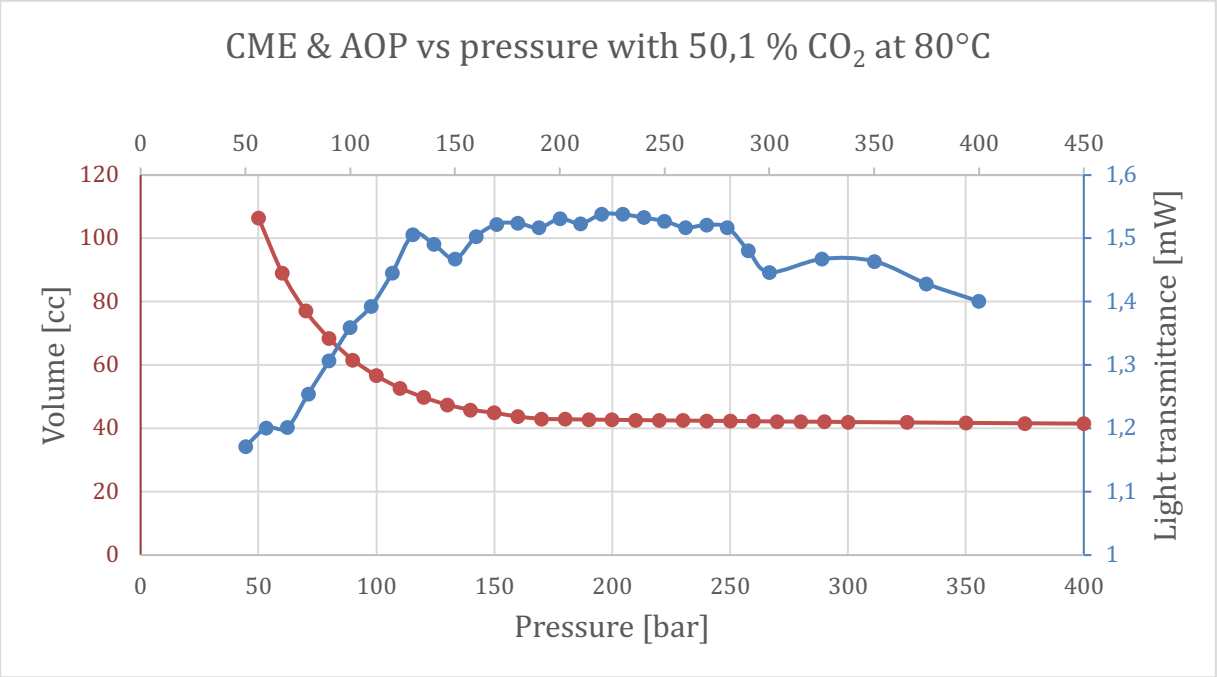

Figure 20 - CME & AOP vs pressure with 50,1 % CO_2 at 80℃

1.13.367 % mole CO_2 added

Originally, we have planned to conduct two tests with different CO_2 content. Unfortunately, due to an unexpected problem with the pump, we didn't manage to hit the original target of a 100% mole ratio of CO_2. After some discussion, we have decided to run one more test with the amount that we have managed to inject into the cell. After calculations, the injected volume turns out to make 67% of the mole ratio. This provided us with one more point for the further modeling part. The test turned out to be a textbook example where we can clearly identify upper and lower AOP. With bubble-point pressure proven to be at 200 bar, upper AOP appears at 270 bar. The trend is again proven: more CO_2 in the system raises both bubble point and AOP. Results are presented in Figure 21.

Internal

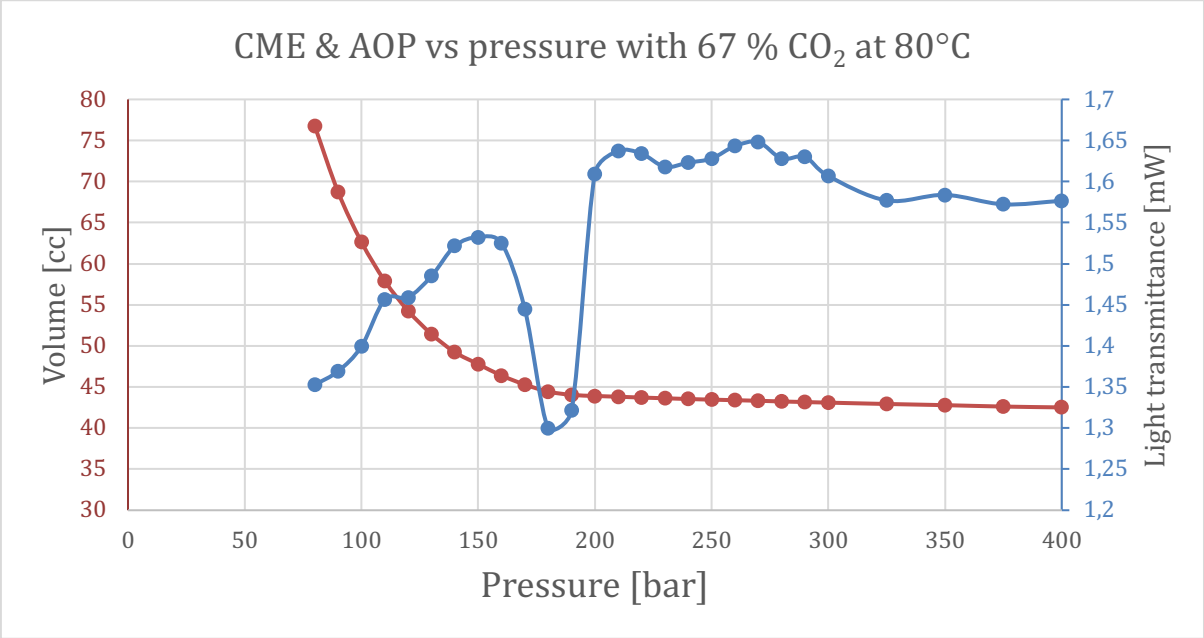

Figure 21 - CME & AOP vs pressure with 67 % CO_2 at 80℃

1.13.4100 % mole CO_2 added

The final test that we have conducted was about adding 100% mole of CO_2 to the sample. The target was hit precisely. In this case, we have expected really high pressure for both bubble-point and AOP, so we set a longer stabilization time before taking reading since the beginning of depressurization of the cell. This ended up with achieving bubble-point pressure equal to 225 bar and AOP at 350 bar. Once again the trend mention previously has been confirmed. Particularly interesting is that we can observe two upper AOP's here. Due to the relatively high bubble point, gas is being released from oil at high pressure. Constant depressurization of the 2-phase system yields another precipitation of asphaltene, appearing after redissolving of particles, due to changes in the liquid composition (after releasing gas). For this test, we have also decided to take pictures using a microscope camera. In order to do so, around 2 cm^2 of fluid needs to be flushed out of the cell so the sample can reach the camera. Pictures were taken at 3 points: before the test (at 400 bar), right above the expected bubble point (at 265 bar) and one at the end of the test (at 50 bar). Photos have been taken constantly for a minute with a few second intervals. At the first point, there were no visible particles. The second point has shown some particles, but they cannot be seen on the still picture (Only when making a time-lapse movie). In the last photo session, there were some particles recognized as well. A not clear indication of asphaltenes on the camera comes from a relatively low amount of asphaltenes (0,9 wt% in STO). Due to removing some volume of sample from the cell, CME data has been corrected for missing volume to produce reliable results. The outcome is presented in Figure 22.

Internal

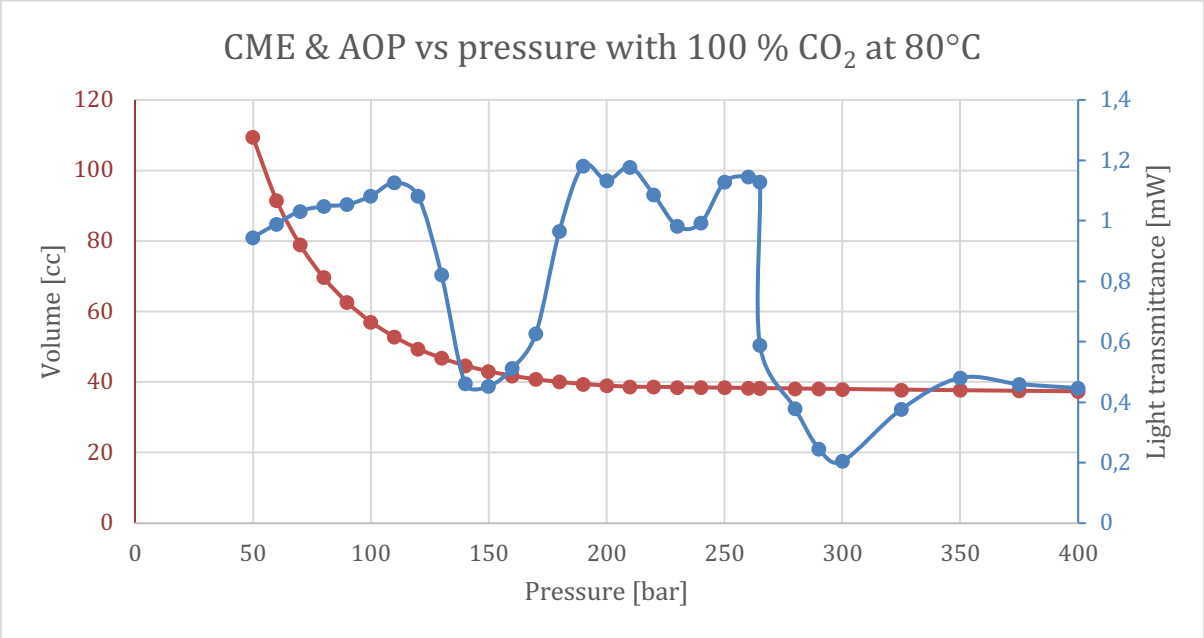

Figure 22 - CME & AOP vs pressure with 100 % CO_2 at 80℃

PVT modeling

1.14 Introduction

The last part of this work is to build a PVT model for a given sample to be able to predict asphaltene precipitation depending on different CO_2 content or temperature during pressure changes. To do this, we have been used PVTsim software, which is not only equipped with tools for building PVT models and tune them based on lab results but also has an asphaltene modeling module. In this section, each step of building such a model is described.

1.15 Composition selection

Firstly, we need to establish the composition and its parameters such as molecular weight, acentric factor, critical temperature, pressure, and obviously mole ratio. We have used composition from C_1 to C_{10+}, where the last one represents all heavy components lumped together. For components from C_1 to C_5, we have used well-established properties. For the rest of the components, molar weight and densities have been also fed to the software to maximize the accuracy of the model.

Internal

1.16 Splitting and lumping

Heavy fraction C_{10+} has been split and then lumped into pseudo-components resulting in 9 pseudo-components. The workflow for lumping is to gather compounds of quite similar properties into one pseudo-component. Such an approach simplifies the computation for the model.

1.17 PVT Tuning

In order to get an accurate fluid model, first, we had to tune it against measured data. We have used results from chromatography and constant mass expansion (For oil sample and mix of oil sample with injection gas (CO_2) in three ratios: 50%, 67%, and 100%). The output of the model before and after tuning is presented in Figure 23 and Figure 24. The most important parameters that mean parameters that have been mostly affected by tuning were critical pressures and temperatures for heavy components and binary interaction coefficients between heavy hydrocarbons and light components or CO_2.

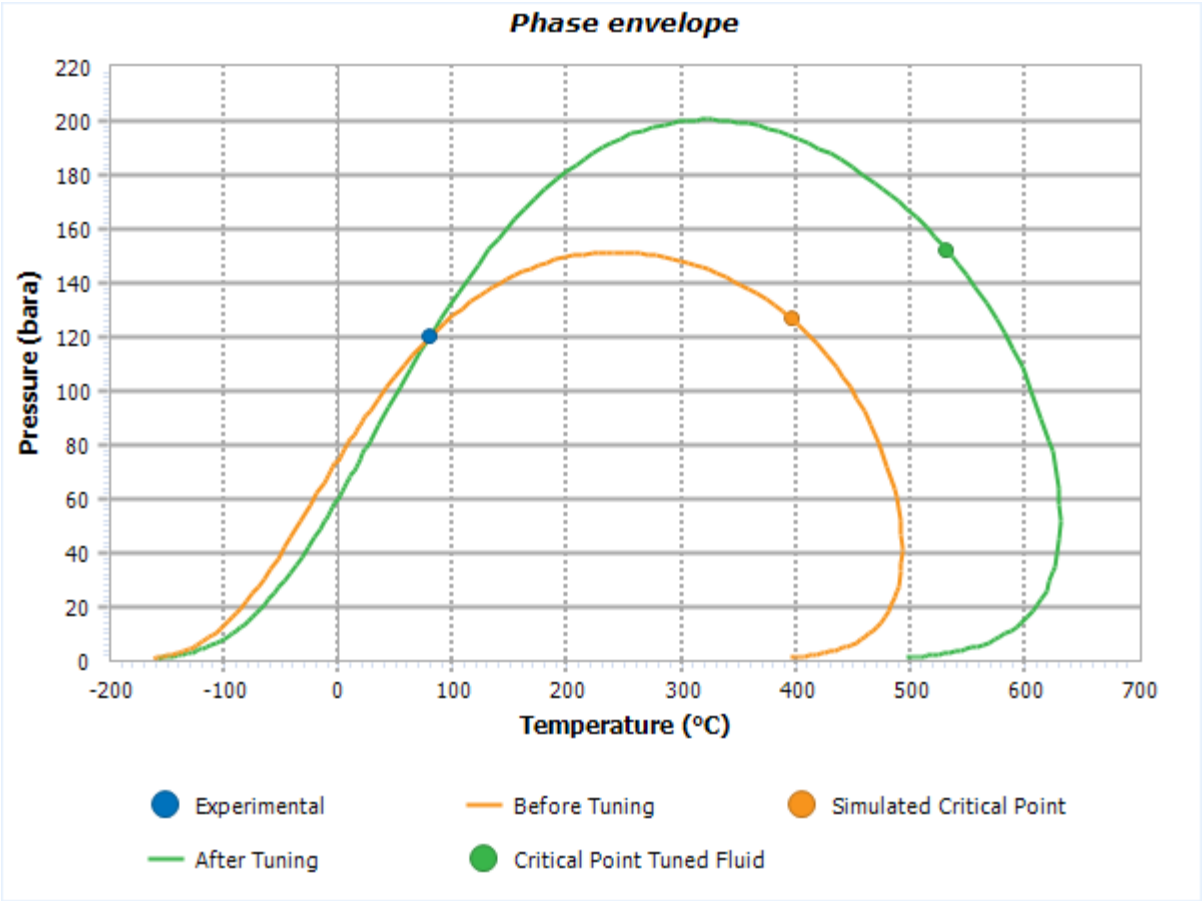

Figure 23 - Phase envelop of fluid model, comparison between models before and after tuning

Internal

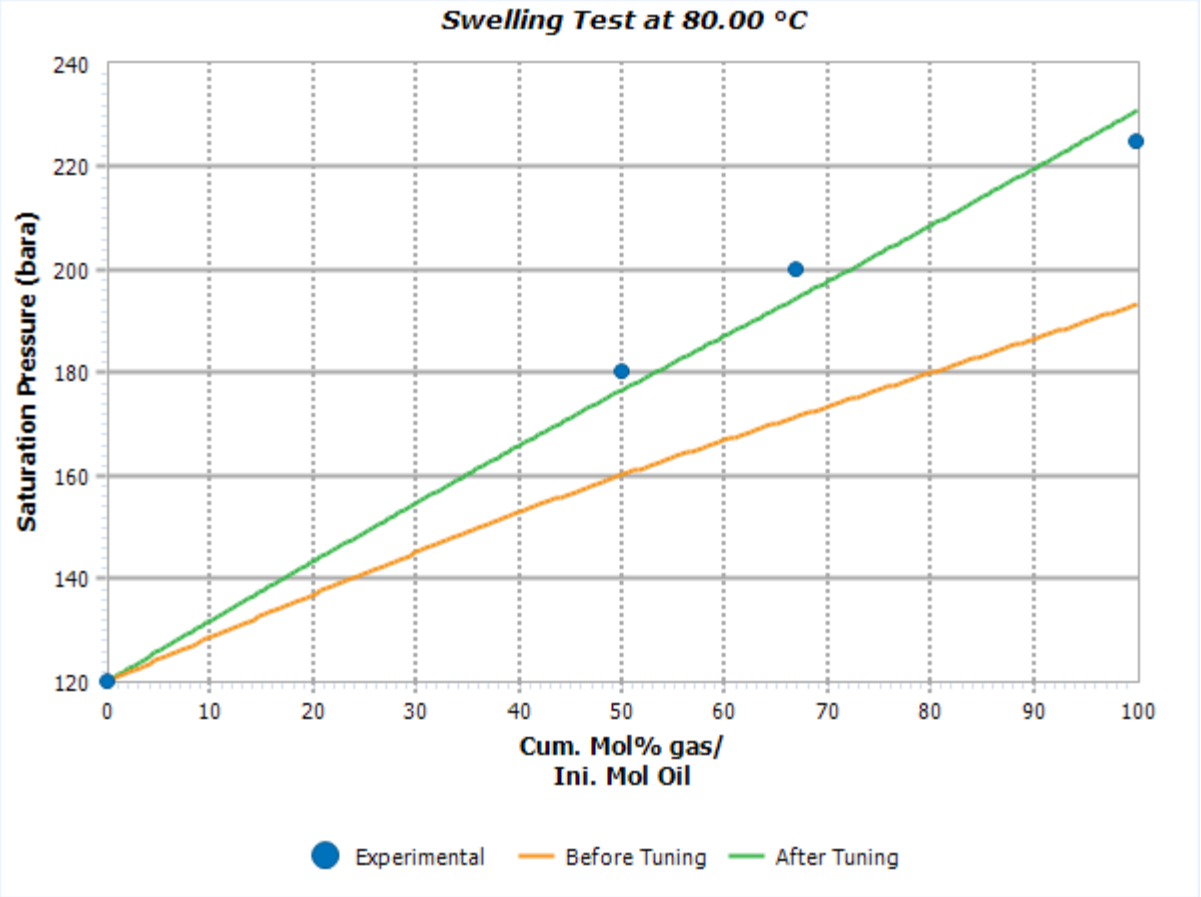

Figure 24 - Swelling test, comparison between models before and after tuning

As we can see, tuning almost perfectly matched the data. This means the model is ready for the next step of modeling.

1.18 AOP modeling

To accurately predict asphaltene onset pressure, It needs to be tuned against the experimental data obtained during laboratory AOP measurements. As mentioned earlier we have identified 4 points, one each for the different ratio of added gas. The overview can be found in Table 6.

CO2 mole ratio [%]	AOP [bar]	Saturation pressure [bar]
0%	140	120
50%	220	180
67%	270	200
100%	350	225

Table 6 - AOP measured data

Internal

At this point, we are introducing the asphaltene component in the composition. In PVTsim be default every component that is above C_{50+} is considered asphaltene. Hence the pseudo-component C_{40-80} has been split into two components, where one of them (marked with the letter "A" represents the asphaltene content. Asphaltene weight percentage (wt%) content has been calculated, and then tuned against the measured data (0,9 wt% from SARA analysis). Input content for the model is represented in mole ratio, hence the weight percentage has been calculated accordingly. The results of asphaltene tuning against measured data (presented in Table 6) have been presented in Figure 26, while Figure 25 represents the model before tuning. At this point, we can only tune properties $_{80}$ (P_c, T_c) of the heaviest component C_{40-80A} and C_{40-80}, and Binary interaction coefficients between C_{40-80A} and non-plus fractions hydrocarbon (C_{1-9}), N_2, and CO_2.

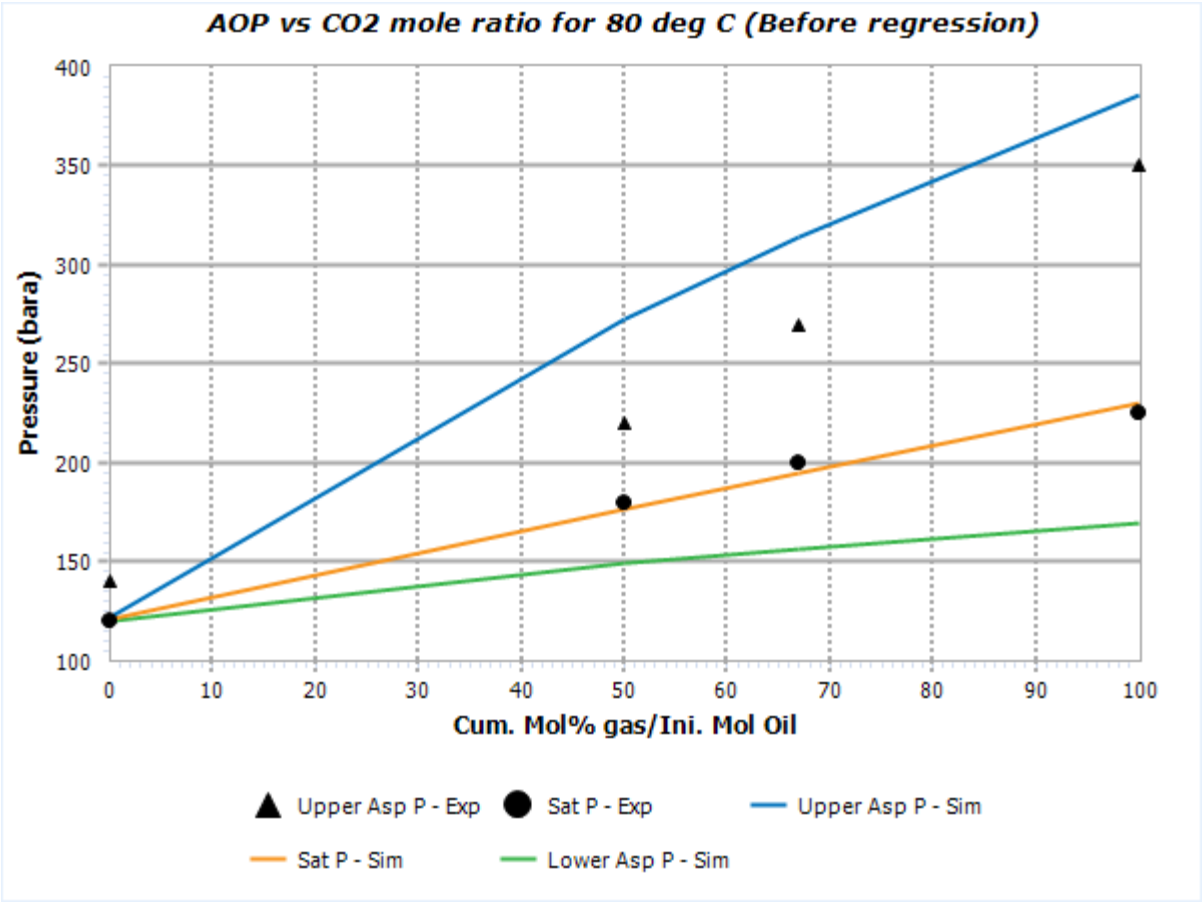

Figure 25- AOP vs CO2 mole ratio for 80 °C, before regression

Internal

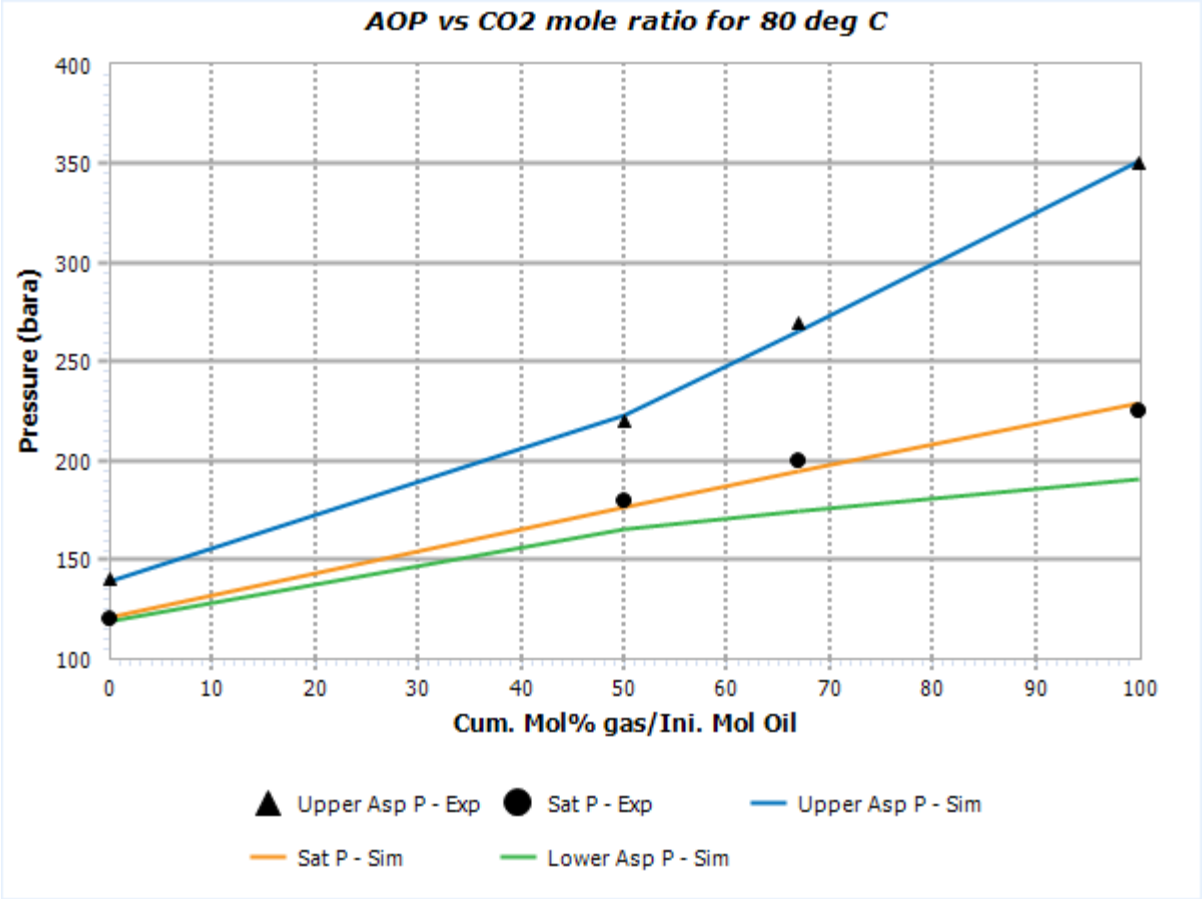

Figure 26 - AOP vs CO2 mole ratio for 80 ℃, after regression

We can clearly notice that supporting the model with experimental data can significantly improve the model. Detailed model parameters have been presented in tables in Appendix 1.25.

1.19 Temperature sensitivity

So far the model has been tuned and yielded results in the same temperature as most of the experiments that took place (80°C). The other measurement in 40°C didn't result in any clear AOP point, hence the model might not be particularly accurate in predicting AOP's for different temperatures (especially lower). Nevertheless, we have run a couple of simulations to see how the asphaltene precipitation is developing in different temperature conditions. All of those models have been simulated for a CO_2 mole ratio varying from 0 to 200%.

Internal

1.19.1 AOP in 80°C

This model extends the previous one to a mole ratio of 200%. As expected with increasing CO_2 in the composition, both asphaltene onset pressure and saturation pressure are increasing.

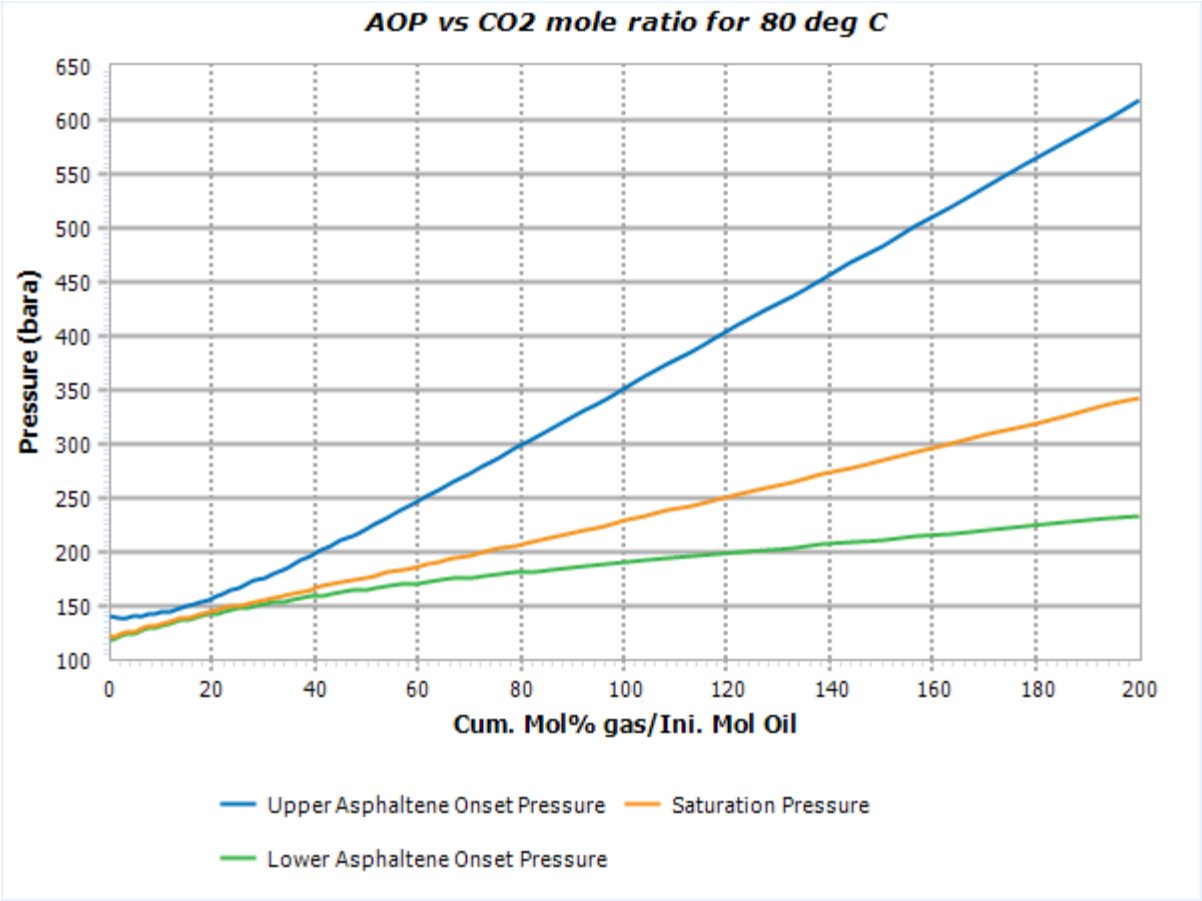

Figure 27 - AOP vs CO2 mole ratio for 80 °C

Internal

1.19.2 AOP in 120°C

Surprisingly the model yielded, what might seems, accurately simulate higher temperature scenarios. We can clearly see that the trend seen in the previous model is observed here. The asphaltene onset pressure is way higher at this temperature. For 0% mole of injected gas, it's twice high as for 80°C (280 bar to 140 bar). However, saturation pressure difference is less significant (146 bar to 120 bar).

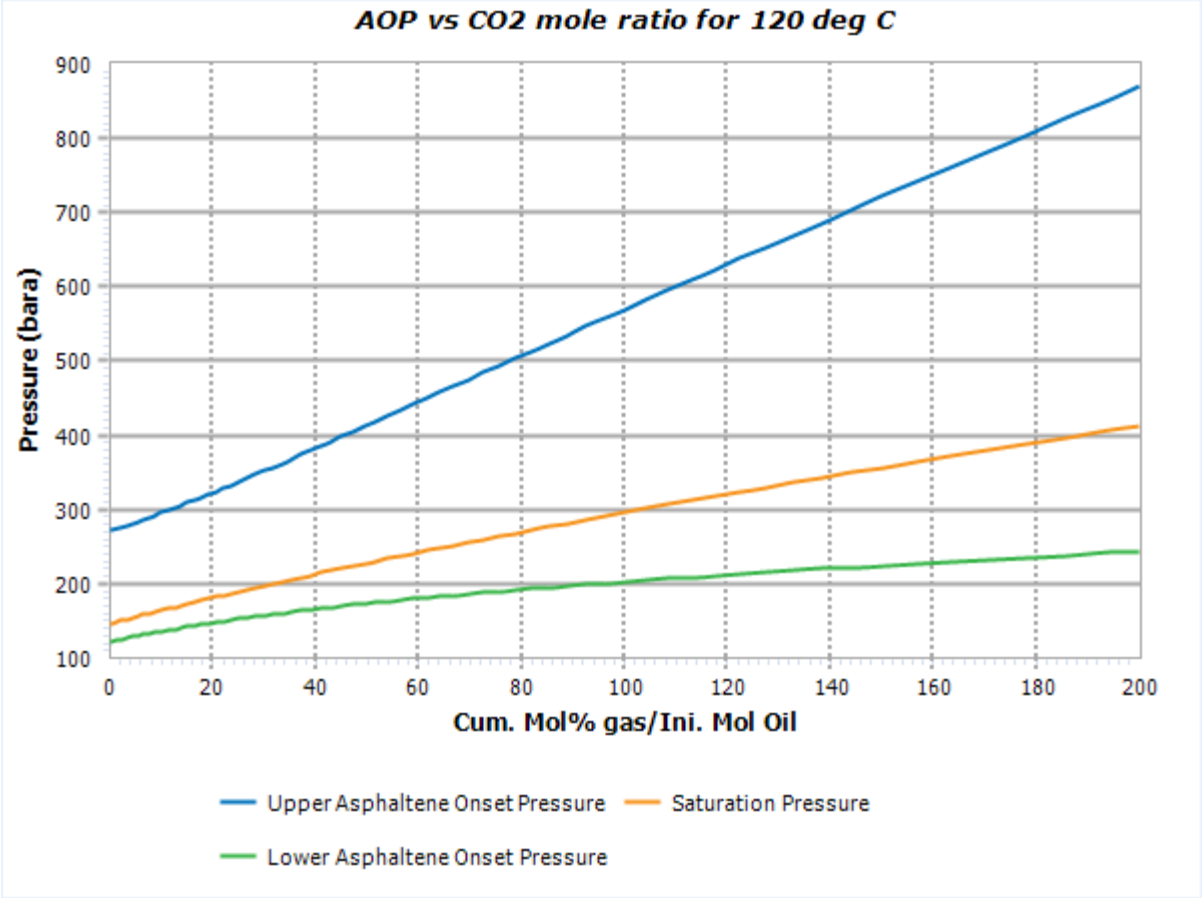

Figure 28 - AOP vs CO2 mole ratio for 120 ℃

Internal

1.19.1 AOP in 40°C

The simulation is questionable. On one hand, we were not able to recognize AOP during measurement in 40°C which seemed not right. However, this has been reproduced on the model, which indicates that for 0% of CO_2 added there is no asphaltene precipitation expected. Running another test at a lower temperature, preferably with and without injection gas added might help indicate the trend and be a good addition to the tuning of the model.

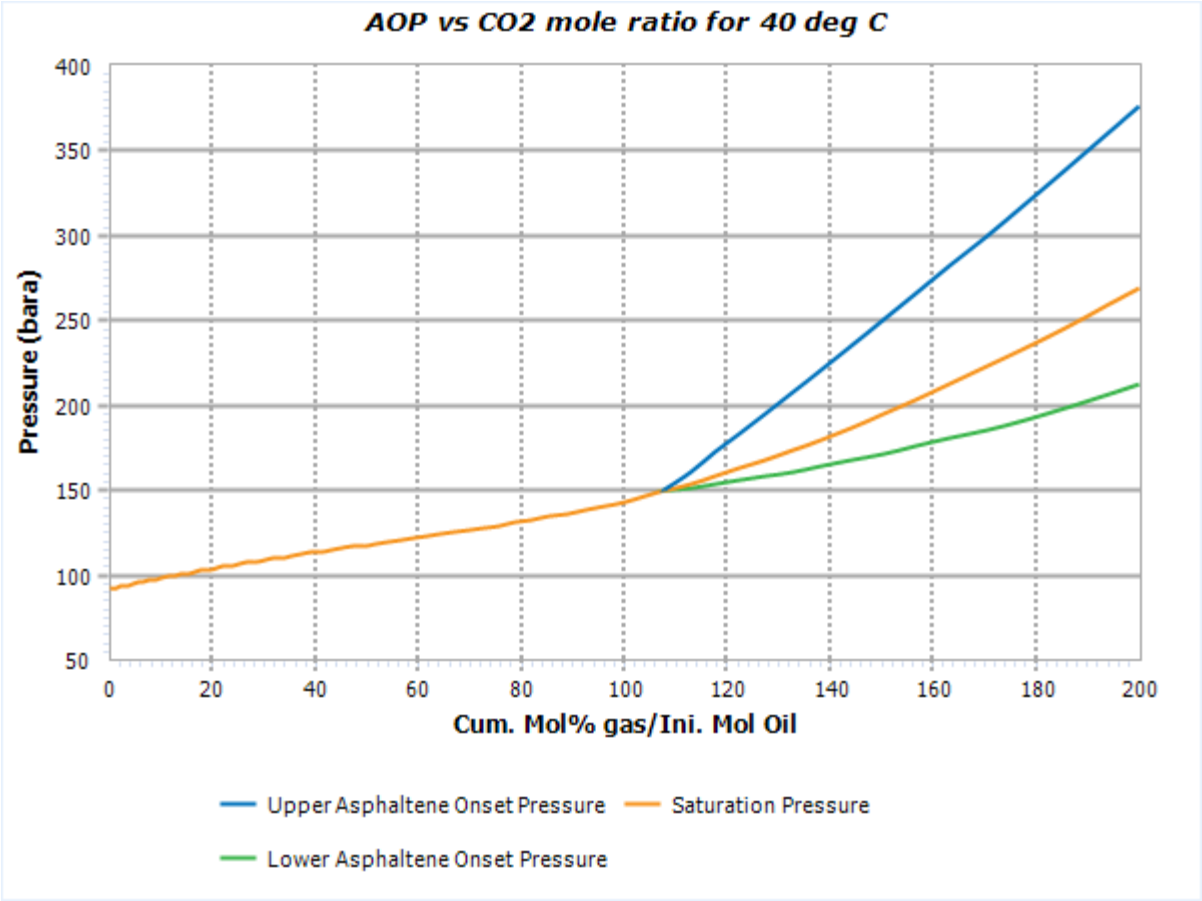

Figure 29 - AOP vs CO2 mole ratio for 40 ℃

Internal

1.20 Discussion

The model was able to reproduce accurately performed measurements and yielded promising simulations for higher temperatures. The biggest uncertainties have occurred during simulating fluid in lower temperatures. Perhaps running additional measurements in lower temperatures could improve the tuning and thus give a more versatile model. Figure 30 represents a comparison of asphaltene onset pressures for different temperatures models. During tuning, we have noticed that the most affected parameters were binary interaction coefficients between asphaltene/non-asphaltene fraction and C_1-C_9 components. That observation suggests prioritizing those parameters during tuning and paying close attention to composition analysis, especially of heavy components.

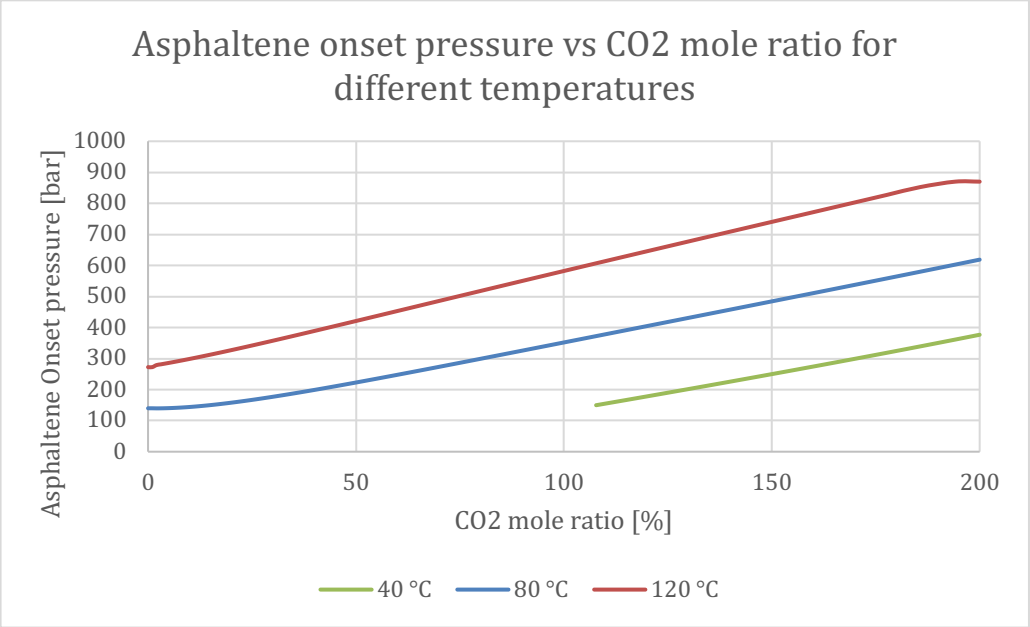

Figure 30 - AOP overview for different temperatures models

Conclusion

Combining laboratory measurements with modeling resulted in great results that have proven the original hypothesis. The CO_2 effect on asphaltene precipitation is significant. The increasing ratio of injected gas to the oil system contributes to the raise of asphaltene onset pressure. Because of higher onset pressure, the asphaltenes might be precipitating directly in the reservoir, which is the highest pressure zone from the whole production chain (reservoir – wellbore – processing plants). This might lead to severe inflow problems and could possibly lead to a significant drop in recovery factor. During the assessment of possible CO_2 injection in future projects, a detailed fluid-injection gas PVT study should be performed to verify possible asphaltene precipitation. For future study, full-field simulation can be studied, which

Internal

could incorporate given above model and check for resulting permeability reduction in the reservoir.

References

[1] W. N. Adyani, W. A. Wan Daud, N. B. Darman, A. I. Memon, I. A. Khan, and A. K. M. Jamaluddin, "A Systematic Approach to Evaluate Asphaltene Precipitation During CO2 Injection," presented at the SPE Enhanced Oil Recovery Conference, Kuala Lumpur, Malaysia, 2011. doi: 10.2118/143903-MS.

[2] H. Lei, S. Pingping, J. Ying, Y. Jigen, L. Shi, and B. Aifang, "Prediction of asphaltene precipitation during CO 2 injection," *Petroleum Exploration and Development*, vol. 37, no. 3, pp. 349–353, Jun. 2010, doi: 10.1016/S1876-3804(10)60038-9.

[3] P. Zanganeh, S. Ayatollahi, A. Alamdari, A. Zolghadr, H. Dashti, and S. Kord, "Asphaltene Deposition during CO2 Injection and Pressure Depletion: A Visual Study," *Energy Fuels*, vol. 26, no. 2, pp. 1412–1419, Feb. 2012, doi: 10.1021/ef2012744.

[4] G. V. Chilingar, *Geology and geochemistry of oil and gas*. Amsterdam; London: Elsevier, 2005.

[5] T. Fan, J. Wang, and J. S. Buckley, "Evaluating Crude Oils by SARA Analysis," in *All Days*, Tulsa, Oklahoma, Apr. 2002, p. SPE-75228-MS. doi: 10.2118/75228-MS.

[6] H. Dembicki, *Practical petroleum geochemistry for exploration and production*. Amsterdam: Elsevier, 2017.

[7] J. A. Duncan, *Asphaltenes characterization, properties, and applications*. New York: Nova Science Publishers, 2010. Accessed: Jan. 21, 2021. [Online]. Available: https://ebookcentral.proquest.com/lib/uvic/detail.action?docID=3018821

[8] S. Alimohammadi, S. Zendehboudi, and L. James, "A comprehensive review of asphaltene deposition in petroleum reservoirs: Theory, challenges, and tips," *Fuel*, vol. 252, pp. 753–791, Sep. 2019, doi: 10.1016/j.fuel.2019.03.016.

[9] J. G. Speight, *The chemistry and technology of petroleum*, 4. ed. Boca Raton, Fla.: Taylor & Francis, 2007.

[10] C. H. Whitson and M. R. Brulé, *Phase behavior*, First. Richardson, Tex: Henry L. Doherty Memorial Fund of AIME, Society of Petroleum Engineers, 2000.

[11] K. S. Pedersen, P. L. Christensen, and J. A. Shaikh, *Phase behavior of petroleum reservoir fluids*, Second edition. Boca Raton: CRC Press, Taylor & Francis Group, 2015.

[12] "Density and density measurement :: Anton Paar Wiki," *Anton Paar*. https://wiki.anton-paar.com/en/density-and-density-measurement/ (accessed Mar. 03, 2021).

[13] D.-Y. Zheng *et al.*, "Theoretical gas phase compressibility factor of mixed refrigerants in auto-cascade refrigeration system," presented at the 5th International Conference on Advanced Design and Manufacturing Engineering, Shenzen, China, 2015. doi: 10.2991/icadme-15.2015.133.

[14] "Vinci Technologies | PVT system for PVT studies & wax / asphaltene precipitation studies | Laboratory and field instruments for Petroleum Industry." https://www.vinci-technologies.com/products-explo.aspx?IDR=82291&idr2=82558&idp=82288&IDM=536790 (accessed May 06, 2021).

[15] "Vinci Technologies | Solid Detection System (SDS) | Laboratory and field instruments for Petroleum Industry." https://www.vinci-technologies.com/products-

Internal

explo.aspx?IDR=113221&idr2=113124&idp=82288&IDM=753562 (accessed May 06, 2021).
[16] "Vinci Technologies | High pressure piston sample cylinder (HPP SERIES) | Laboratory and field instruments for Petroleum Industry." https://www.vinci-technologies.com/products-explo.aspx?IDM=753797&IDR=113222&IDR2=113224 (accessed May 05, 2021).

Appendix

1.21 Z-factor calculations

Soave-Redlich-Kwong equation of the state

$$z^3 - z^2 + (A - B + B^2) \cdot z - AB = 0 \quad (4)$$

Where

Parameter A:

$$A = \frac{a(T) \cdot P}{R^2 \cdot T^2} \quad (5)$$

Parameter B:

$$B = \frac{b \cdot P}{R \cdot T} \quad (6)$$

Parameter a(T):

$$a(T) = a_c \cdot \alpha(T) \quad (7)$$

Parameter a_c:

$$a_c = \frac{0{,}42747 \cdot R^2 \cdot {T_c}^2}{P_c} \quad (8)$$

Parameter b:

$$b = \frac{0{,}08664 \cdot R \cdot T_c}{P_c} \quad (9)$$

Parameter $\alpha(T)$:

$$\alpha(T) = \left(1 + m\left(1 - \sqrt{\frac{T}{T_c}}\right)\right)^2 \quad (10)$$

Parameter m (based on acentric factor):

$$m = 0{,}480 + 1574 \cdot \omega - 0{,}176\omega^2 \quad (11)$$

After calculating all the parameters (5-11), the Newton-Raphson iterative method is introduced with equation 11:

$$z_2 = z_1 - \frac{F(z_1)}{F_{z_1}(z_1)} \quad (12)$$

Internal

Combining equation 3 with equation 11 yields equation 12:

$$F(z_1) = z^3 - z^2 + (A - B + B^2) \cdot z - AB = 0 \text{ (13)}$$

Precision factor ε must be introduced to establish sufficient result and end of iteration process:

$$\varepsilon > |z_1 - z_2| \text{ (14)}$$

Calculation procedure:

1. The initial guess of z_0 is set (usually 1) and precision factor ε.
2. Calculating z_2 using equation 12
3. If equation 14 returns true proceed to the next step, otherwise new $z_0 = z_1$

   Z_1 is the calculated compressibility factor.

Internal

1.22 Separator sample total composition

	Stock tank gas		Stock tank oil		Recombined fluid	
Component	**Mole %**	**Weight %**	**Mole %**	**Weight %**	**Mole %**	**Weight %**
Nitrogen	1,973	1,165	-	-	0,140	0,021
Carbon dioxide	0,808	0,750	-	-	0,057	0,014
Hydrogen Sulphide	0,000	0,000	-	-	0,000	0,000
Methane	11,724	3,963	0,012	0,001	0,844	0,073
Ethane	14,399	9,123	0,182	0,028	1,192	0,193
Propane	32,198	29,917	1,689	0,380	3,856	0,917
iso-Butane	7,148	8,754	0,907	0,269	1,350	0,423
n-Butane	15,194	18,608	3,035	0,900	3,898	1,222
Neopentane	0,124	0,189	0,038	0,014	0,044	0,017
iso-Pentane	4,606	7,002	2,197	0,809	2,368	0,922
n-Pentane	4,886	7,429	3,257	1,199	3,373	1,312
Hexanes	3,317	5,901	5,376	2,330	5,230	2,395
Heptanes	2,545	4,808	8,888	4,157	8,437	4,169
Octanes	0,929	2,009	10,212	5,482	9,553	5,419
Nonanes	0,122	0,304	7,026	4,277	6,536	4,205
Decanes	0,027	0,077	6,008	4,108	5,583	4,035
Undacanes	0,001	0,002	4,583	3,438	4,258	3,376
Dodecanes	0,000	0,000	3,806	3,127	3,536	3,070
Tridecanes	0,000	0,000	3,950	3,527	3,669	3,463
Tetradecanes	0,000	0,000	3,370	3,267	3,130	3,208
Pentadecanes	0,000	0,000	3,548	3,730	3,296	3,662
Hexadecanes	0,000	0,000	2,883	3,266	2,678	3,207
Heptadecanes	0,000	0,000	2,543	3,076	2,363	3,020
Octadecanes	0,000	0,000	2,593	3,321	2,409	3,261
Nonadecanes	0,000	0,000	2,088	2,802	1,940	2,751
Eicosanes	0,000	0,000	1,763	2,474	1,638	2,429
C21	0,000	0,000	1,605	2,384	1,491	2,341
C22	0,000	0,000	1,458	2,232	1,354	2,191
C23	0,000	0,000	1,352	2,152	1,256	2,113
C24	0,000	0,000	1,211	2,002	1,125	1,966
C25	0,000	0,000	1,114	1,916	1,035	1,881
C26	0,000	0,000	1,028	1,830	0,955	1,797
C27	0,000	0,000	0,964	1,771	0,896	1,739
C28	0,000	0,000	0,895	1,699	0,831	1,668
C29	0,000	0,000	0,870	1,695	0,808	1,664
C30	0,000	0,000	0,806	1,621	0,749	1,592
C31	0,000	0,000	0,733	1,512	0,681	1,485
C32	0,000	0,000	0,655	1,388	0,609	1,363
C33	0,000	0,000	0,571	1,242	0,531	1,219
C34	0,000	0,000	0,503	1,121	0,467	1,101

Internal

	Stock tank gas		Stock tank oil		Recombined fluid	
Component	**Mole %**	**Weight %**	**Mole %**	**Weight %**	**Mole %**	**Weight %**
C35	0,000	0,000	0,468	1,063	0,435	1,044
C36+	0,000	0,000	5,813	18,390	5,400	18,056
Sum	100,000	100,000	100,000	100,000	100,000	100,000
Average molecular weight:		47,46		196,0		185,416061
Gas gravity:	1,638					

Internal

1.23 Recombined sample total composition

Component	Stock tank gas		Stock tank oil		Recombined fluid	
	Mole %	Weight %	Mole %	Weight %	Mole %	Weight %
Nitrogen	0,833	0,847	-	-	0,376	0,087
Carbon dioxide	3,204	5,117	-	-	1,447	0,523
Hydrogen Sulphide	0,000	0,000	-	-	0,000	0,000
Methane	63,748	37,106	0,149	0,012	28,866	3,803
Ethane	9,831	10,726	0,292	0,044	4,599	1,136
Propane	9,482	15,170	1,225	0,271	4,953	1,794
iso-Butane	2,807	5,920	0,923	0,269	1,774	0,847
n-Butane	5,392	11,372	2,867	0,836	4,007	1,913
Neopentane	0,035	0,091	0,008	0,003	0,020	0,012
iso-Pentane	1,171	3,066	1,566	0,567	1,388	0,822
n-Pentane	1,327	3,475	2,544	0,921	1,995	1,182
Hexanes	0,992	3,038	5,004	2,132	3,192	2,225
Heptanes	0,789	2,565	8,942	4,117	5,261	3,958
Octanes	0,314	1,171	10,533	5,560	5,919	5,111
Nonanes	0,053	0,227	7,282	4,357	4,018	3,935
Decanes	0,018	0,086	6,220	4,182	3,420	3,763
Undacanes	0,004	0,023	4,706	3,471	2,583	3,119
Dodecanes	0,000	0,001	3,921	3,167	2,150	2,843
Tridecanes	0,000	0,000	4,081	3,583	2,238	3,217
Tetradecanes	0,000	0,000	3,463	3,301	1,899	2,964
Pentadecanes	0,000	0,000	3,620	3,741	1,985	3,359
Hexadecanes	0,000	0,000	2,978	3,317	1,633	2,978
Heptadecanes	0,000	0,000	2,566	3,051	1,407	2,739
Octadecanes	0,000	0,000	2,681	3,376	1,470	3,031
Nonadecanes	0,000	0,000	2,133	2,815	1,170	2,527
Eicosanes	0,000	0,000	1,811	2,498	0,993	2,243
C21	0,000	0,000	1,641	2,396	0,900	2,151
C22	0,000	0,000	1,464	2,203	0,803	1,978
C23	0,000	0,000	1,389	2,174	0,762	1,952
C24	0,000	0,000	1,219	1,981	0,668	1,779
C25	0,000	0,000	1,135	1,919	0,622	1,723
C26	0,000	0,000	1,042	1,824	0,571	1,638
C27	0,000	0,000	0,966	1,744	0,530	1,566

Internal

Component	Stock tank gas		Stock tank oil		Recombined fluid	
	Mole %	Weight %	Mole %	Weight %	Mole %	Weight %
C28	0,000	0,000	0,905	1,689	0,496	1,516
C29	0,000	0,000	0,871	1,670	0,478	1,499
C30	0,000	0,000	0,812	1,606	0,446	1,442
C31	0,000	0,000	0,742	1,503	0,407	1,349
C32	0,000	0,000	0,649	1,351	0,356	1,213
C33	0,000	0,000	0,572	1,222	0,314	1,097
C34	0,000	0,000	0,516	1,132	0,283	1,016
C35	0,000	0,000	0,476	1,062	0,261	0,953
C36+	0,000	0,000	6,087	18,933	3,338	16,998
Sum	100,000	100,000	100,000	100,000	100,000	100,000
Average molecular weight:	-	27,56	-	199,3	-	121,76118
Gas gravity:	0,952		-		-	-

Internal

1.24 Simple composition

Composition of reservoir fluid				
Component	**Mole [%]**	**Weight [%]**	**Molar Weight**	**Density [kg/m³]**
Nitrogen	0,376	0,087	28,02	804,0
Carbon Dioxide	1,447	0,523	44,01	809,0
Hydrogen Sulphide	0,000	0,000	34,08	797,0
Methane	28,866	3,803	16,04	300,0
Ethane	4,599	1,136	30,07	356,7
Propane	4,953	1,794	44,09	506,7
iso-Butane	1,774	0,847	58,12	562,1
n-Butane	4,007	1,913	58,12	583,1
Neopentane	0,020	0,012	72,15	597,0
iso-Pentane	1,388	0,822	72,15	623,3
n-Pentane	1,995	1,182	72,15	629,9
Hexanes, C6 total	**3,192**	**2,225**	**84,8**	**667,0**
n-Hexane	1,478	1,046	86,2	662,7
iso-Paraffins (C6)	1,451	1,027	86,2	660,7
Naphtenes (C6)	0,264	0,152	70,1	748,1
Heptanes, C7 total	**5,261**	**3,958**	**91,6**	**738,2**
n-Heptane	1,198	0,986	100,2	686,9
iso-Paraffins (C7)	0,959	0,789	100,2	688,0
Naphtenes (C7)	2,470	1,777	87,6	766,0
Aromatics (C7)	0,634	0,407	78,1	883,1
Octanes, C8 total	**5,919**	**5,111**	**105,1**	**760,4**
n-Octane	0,927	0,870	114,2	707,0
iso-Paraffins (C8)	0,960	0,905	114,9	707,6
Naphtenes (C8)	3,068	2,607	103,5	772,1
Aromatics (C8)	0,964	0,729	92,1	872,0
Nonanes, C9 total	**4,018**	**3,935**	**119,2**	**777,9**
n-Nonane	0,800	0,843	128,3	723,0
iso-Paraffins (C9)	0,934	0,985	128,4	723,3
Naphtenes (C9)	1,042	1,024	119,7	793,8
Aromatics (C9)	1,241	1,083	106,2	872,9
Decanes plus, C10+	**32,184**	**72,653**	**275**	**885**
Sum	100,000	100,000	-	-
Average molecular weight:	-	-	121,761284	-
Gas gravity:	-	-	-	-

Internal

1.25 PVT model parameters

Component	Mol [%]	Molecular Weight	Liquid Density [g/cm³]	Critical Temperature [°C]	Critical Pressure [bara]	Acentric Factor	Normal Tb[°C]	Weight Av. Molecular Weight
N2	0,36985	28,013521		-146,9500031	33,9438711	0,04	-195,75001	28,01351929
CO2	1,42333	44,0098		31,05001221	73,7646031	0,225	-78,500006	44,00979614
C1	28,3938	16,042879		-82,5499939	46,0015477	0,008	-161,55001	16,0428791
C2	4,52377	30,06982		32,2499939	48,8386508	0,098	-88,549994	30,0698204
C3	4,87198	44,09676		96,64998779	42,4551804	0,152	-42,049994	44,09676361
iC4	1,71593	58,123699		134,9499756	36,4770077	0,176	-11,750006	58,12369919
nC4	3,94145	58,123695		152,0500122	37,9968789	0,193	-0,4499878	58,123703
neo-C5	0,01935	72,151001		160,6499878	32,0187004	0,197	9,4500061	72,15100098
iC5	1,36529	72,150642		187,2499939	33,8425515	0,227	27,85	72,1506424
nC5	1,96237	72,150642		196,4499756	33,7412204	0,251	36,050012	72,1506424
C6	3,13978	84,800003	0,666999996	234,2499939	29,6882223	0,296	68,749994	86,17758179
C7	5,17494	91,599998	0,738200009	361,021936	38,9653268	0,364058	91,950006	91,59999847
C8	5,82218	105,09999	0,760399997	389,7661987	34,4714805	0,395507	116,74999	105,1000061
C9	3,95227	119,2	0,777899981	416,0830322	30,8655808	0,427821	142,24999	119,1999893
C10-C12	9,0067	146,39104	0,803411305	460,7331787	26,1522081	0,49022	186,9634	147,2146912
C13-C14	4,60809	182,10677	0,830447733	509,7312866	22,5913558	0,56574	236,74093	182,4148102
C15-C16	3,73555	213,58054	0,848430634	547,935083	20,6276428	0,629934	274,22183	213,8793793
C17-C19	4,31999	249,42413	0,867596447	588,0278564	19,2521694	0,699346	312,07711	249,8766479
C20-C22	3,15306	289,28442	0,887721598	629,3474365	18,3428538	0,77105	350,07473	289,8032532
C23-C26	2,92094	336,45956	0,90750891	674,6269775	17,6392329	0,848155	390,46511	337,148468
C27-C31	2,2861	399,07507	0,929209769	730,3819824	17,0712008	0,936118	436,00515	400,0434265
C32-C39	1,88207	485,37601	0,954520524	802,2392822	16,709905	1,027255	486,14858	487,4222412
C40-C80	1,26703	674,63818	0,986897767	849,9312988	17,4008808	1,026955	581,30709	694,199646
C40-C80-A	0,14418	674,63818	1,109122992	2567,711572	8,588474	1,274	581,30709	694,199646

Internal

Component	Critical Volume [cm³/mol]	Vapor Pressure Model	M & C C1	M & C C2	M & C C3
N2	89,8	Classic	0,542699993	-0,0524	-0,3381
CO2	94	Classic	0,8653	-0,438600004	1,34469998
C1	99	Classic	0,585699975	-0,720600009	1,28989995
C2	148	Classic	0,717800021	-0,764400005	1,63960016
C3	203	Classic	0,786300004	-0,745899975	1,84539998
iC4	263	Classic	0,239999995	3,835999966	-8,0450001
nC4	255	Classic	0,878700018	-0,939899981	2,26659989
neo-C5	303	Classic	0,783248007	0	0
iC5	306	Classic	0,82822901	0	0
nC5	304	Classic	1,027999997	-2,562000036	6,24800014
C6	370	Classic	0,930483997	0	0
C7	456,813	Classic			
C8	485,447	Classic			
C9	525,004	Classic			
C10-C12	620,376	Classic			
C13-C14	753,127	Classic			
C15-C16	883,925	Classic			
C17-C19	1040,69	Classic			
C20-C22	1222,06	Classic			
C23-C26	1447,41	Classic			
C27-C31	1759,37	Classic			
C32-C39	2211,12	Classic			
C40-C80	3346,1	Classic			
C40-C80-A	3346,1	Classic			

Internal

Component	Cpen [cm³/mol]	CpenT [cm³/(mol ºC)]	Href [J/mol]	1. Cp-con[J/mol °C]	2. Cp-con [J/mol ºC^2]	3. Cp-con [J/mol C^3]	4. Cp-con [J/mol C^4]
N2	0,92	0	8330,78904	31,14884443	-0,0135648	2,68E-05	-1,17E-08
CO2	3,028	0,006688	19459,10309	19,79458723	0,07343423	-5,60E-05	1,72E-08
C1	0,63	0	2,642503837	19,25031915	0,05212407	1,20E-05	-1,13E-08
C2	2,63	0	9761,134731	5,409180871	0,17810104	-6,94E-05	8,71E-09
C3	5,06	0	19519,62239	-4,224351809	0,30625508	-0,00016	3,21E-08
iC4	7,29	0	29278,12121	-1,38997505	0,38471325	-0,00018	2,90E-08
nC4	7,86	0	29278,11918	9,486998168	0,33129138	-0,00011	-2,82E-09
neo-C5	9,68	0	39036,60989	-16,59177682	0,55515273	-0,00033	7,63E-08
iC5	10,93	0	39036,60989	-9,524680355	0,50658716	-0,00027	5,72E-08
nC5	12,18	0	39036,60989	-3,625658566	0,48732868	-0,00026	5,30E-08
C6	17,98	0	48795,10262	-4,412752334	0,58194728	-0,00031	6,49E-08
C7	7,582	-0,0454787	52567,15215	-3,260191066	0,52957456	-0,0002	0
C8	15,6357	-0,0488719	61959,0132	-2,417074818	0,59752147	-0,00023	0
C9	23,7804	-0,0542614	71768,28344	-0,512958266	0,66847094	-0,00027	0
C10-C12	37,2146	-0,0684438	90684,92754	1,654716025	0,81839112	-0,00033	0
C13-C14	48,3198	-0,0895605	115532,1178	2,724862564	1,0121519	-0,00041	0
C15-C16	53,1212	-0,1109101	137428,2122	3,497577838	1,18870463	-0,00048	0
C17-C19	52,5774	-0,1350177	162364,3635	4,109698526	1,38849569	-0,00057	0
C20-C22	45,7855	-0,1604985	190094,93	3,862014993	1,6089545	-0,00066	0
C23-C26	32,7548	-0,1902189	222914,3548	3,69104881	1,87128935	-0,00076	0
C27-C31	9,44092	-0,2280639	266475,5501	3,388085697	2,21900496	-0,00091	0
C32-C39	-30,6247	-0,2756914	326514,5427	1,90836778	2,69675159	-0,00111	0
C40-C80	-205,283	-0,3775543	458183,2616	-1,3985511	3,82461455	-0,00157	0
C40-C80-A	1790,45	-0,2494122	458183,2616	-1,3985511	3,82461455	-0,00157	0

Internal

Component	Melting Temp Tf [°C]	Hf [J/mol]	Paraffinic Fraction	Naphthenic Fraction	Aromatic Fraction	Wax Fraction	Asphaltene Fraction
N2							
CO2							
C1							
C2							
C3							
iC4							
nC4							
neo-C5	-16,55						
iC5							
nC5							
C6							
C7	-116,471	8562,824004	0,491528809	0,3833636	0,125108	0,3388057	0
C8	-87,831	11620,74155	0,517357767	0,35047171	0,132171	0,2997884	0
C9	-64,7587	14820,63982	0,538194239	0,32654172	0,135264	0,2746926	0
C10-C12	-33,1488	21067,08174	0,558142126	0,30030692	0,141551	0,2429514	0
C13-C14	-4,79023	29191,92694	0,548723102	0,29020754	0,161069	0,2071518	0
C15-C16	12,3823	36411,11209	0,533466935	0,29239377	0,174139	0,1832001	0
C17-C19	26,8014	44632,94691	0,555791855	0,26123133	0,182977	0,155505	0
C20-C22	38,9863	53843,11812	0,549084008	0,2524983	0,198418	0,1240993	0
C23-C26	49,8598	64661,82824	0,537010252	0,24704827	0,215942	0,0908297	0
C27-C31	60,5107	78673,0902	0,517908275	0,24368492	0,238407	0,0501736	0
C32-C39	68,4559	92008,05767	0,487811387	0,24201939	0,270169	0,0065458	0
C40-C80	89,6168	150849,2907	0,51518625	0,27028045	0,214533	0	0
C40-C80-A	89,6168	150849,2907	0	0	1	0	1

Internal

Component	Component Type	Forms Hydrates	Crit. Pres. Wax [bara]	Omega A	Omega B
N2	Inorganic	I & II & H		0,427480012	0,08663999
CO2	Inorganic	I & II		0,427480012	0,08664
C1	Organic Defined	I & II & H		0,427480012	0,08664
C2	Organic Defined	I & II		0,427480012	0,08664
C3	Organic Defined	II		0,427480012	0,08664
iC4	Organic Defined	II		0,427480012	0,08664
nC4	Organic Defined	II		0,427480012	0,08664
neo-C5	Organic Defined	II		0,427480012	0,08663999
iC5	Organic Defined	H		0,427480042	0,08664
nC5	Organic Defined	None		0,427479982	0,08664
C6	Organic Defined	None		0,427480012	0,08664
C7	C7+ Pseudo	None	34,00641075	0,427480221	0,08664035
C8	C7+ Pseudo	None	30,08447338	0,427480221	0,08664035
C9	C7+ Pseudo	None	26,93747837	0,427480251	0,08664035
C10-C12	C7+ Pseudo	None	22,88915918	0,427480221	0,08664035
C13-C14	C7+ Pseudo	None	19,73125839	0,427480251	0,08664035
C15-C16	C7+ Pseudo	None	18,01352552	0,427480221	0,08664034
C17-C19	C7+ Pseudo	None	16,81686013	0,427480251	0,08664035
C20-C22	C7+ Pseudo	None	12,25363465	0,427480191	0,08664034
C23-C26	C7+ Pseudo	None	9,276919019	0,427480221	0,08664035
C27-C31	C7+ Pseudo	None	8,71669954	0,427480221	0,08664035
C32-C39	C7+ Pseudo	None	8,354035478	0,427480251	0,08664035
C40-C80	C7+ Pseudo	None	7,711312892	0,427480221	0,08664035
C40-C80-A	C7+ Pseudo	None	7,711312892	0,427480221	0,08664035

Internal

Component	A I Small HV [°C/bar]	B I Small HV K	A I Large HV [°C/bar]	B I Large HV K	A II Small [HV °C/bar]	B II Small HV K	A II Large [HV °C/bar]
N2	0,0528	932,29999	0,03414755	2240	0,007507	2004	0,09477
CO2	1,03E-12	8311,2656	0,321546161	2334,337891	6,08E-05	3691	0,1683
C1	0,04792	1594	0,01243523	2952	0,002317	2777	1,0759999
C2	0	0	0,00299926	3861	0	0	0,007362
C3					0	0	0,008264
iC4					0	0	0,08189
nC4					0	0	0,001262
neo-C5					0	0	0,0005472
iC5							
nC5							

Component	B II Large HV K	A H Small [HV °C/bar]	B H Small HV K	A H Medium HV [°C/bar]	B H Medium HV K	A H Huge HV [°C/bar]	B H Huge HV K
N2	1596	1,32E-05	3795	0	0		
CO2	2591			0	0		
C1	1323	0,0002763	3390	0	0		
C2	4000			0	0		
C3	4521			0	0		
iC4	4013			0	0		
nC4	4580			0	0		
neo-C5	5570						
iC5				0	0	16394,9	1699
nC5				0	0		

Internal

Binary Interaction coefficient

	N2	CO2	C1	C2	C3	iC4	nC4	neo-C5	iC5	nC5	C6	C7	C8	C9	C10-C12	C13-C14	C15-C16	C17-C19	C20-C22	C23-C26	C27-C31	C32-C39	C40-C80	C40-C80-A
N2	X																							
CO2	-0,031500001	X																						
C1	0,027799999	0,119999997	X																					
C2	0,0407	0,119999997	0	X																				
C3	0,076300003	0,120000005	0	0	X																			
iC4	0,094400004	0,119999997	0	0	0	X																		
nC4	0,069999993	0,120000005	0	0	0	0	X																	
neo-C5	0	0	0	0	0	0	0	X																
iC5	0,0867	0,119999997	0	0	0	0	0	0	X															
nC5	0,087800004	0,120000012	0	0	0	0	0	0	0	X														
C6	0,079999998	0,119999997	0	0	0	0	0	0	0	0	X													
C7	0,079999991	0,086050302	-0,100000001	0	0	0	0	0	0	0	0	X												
C8	0,079999998	0,086050302	-0,100000001	0	0	0	0	0	0	0	0	0	X											
C9	0,079999998	0,086050309	-0,100000001	0	0	0	0	0	0	0	0	0	0	X										
C10-C12	0,079999998	0,086050294	-0,100000001	0	0	0	0	0	0	0	0	0	0	0	X									
C13-C14	0,079999998	0,086050302	-0,100000001	0	0	0	0	0	0	0	0	0	0	0	0	X								
C15-C16	0,079999998	0,086050294	-0,100000001	0	0	0	0	0	0	0	0	0	0	0	0	0	X							
C17-C19	0,079999991	0,086050302	-0,100000001	0	0	0	0	0	0	0	0	0	0	0	0	0	0	X						
C20-C22	0,080000006	0,086050302	-0,100000001	0	0	0	0	0	0	0	0	0	0	0	0	0	0	0	X					
C23-C26	0,079999991	0,086050302	-0,100000001	0	0	0	0	0	0	0	0	0	0	0	0	0	0	0	0	X				
C27-C31	0,079999991	0,086050302	-0,100000001	0	0	0	0	0	0	0	0	0	0	0	0	0	0	0	0	0	X			
C32-C39	0,079999991	0,086050317	-0,100000001	0	0	0	0	0	0	0	0	0	0	0	0	0	0	0	0	0	0	X		
C40-C80	0,079999991	0,086050272	-0,100000001	0	0	0	0	0	0	0	0	0	0	0	0	0	0	0	0	0	0	0	X	
C40-C80-A	0,079999991	0,058240939	0,04310197	0,017155439	0,019051287	0,017000001	0,017000001	0	0,017000001	0,017000001	0,017000001	0,017000001	0,017000001	0,017000001	0	0	0	0	0	0	0	0	0	X

Internal